1

Fundamentals of Organic Light-Emitting Diode

Chin H. Chen[1,2]

[1]*Shine Materials Technology Co., Ltd., Kaohsiung, Taiwan, Republic of China*
[2]*Shanghai Taoe Chemical Technology Co., Ltd., Shanghai, P.R. China*

1.1 Brief History

Organic electroluminescence (EL) is the electrically driven light-emitting phenomenon of organic materials first reported by Pope in 1963 [1, 2], who had discovered that by applying a high DC voltage (>100 V) across a thick layer (10–20 μm) of anthracene crystals sandwiched between two electrodes of Ag (epoxy paste), a faint blue EL could be detected. But, the high voltage required for charge injection prohibited any consideration for practical application. In order to reduce the driving voltage and to improve the luminance efficiency, much effort has been spent ever since [3, 4].

It was not until 1987, a small research team led by Tang at Kodak [5] realized the first practical organic light-emitting diode (OLED) with a *p*–*n* heterojunction, which consisted of a double thin-layer structure of a *p*-type electron donor molecule of TAPC and an *n*-type electron acceptor molecule of Alq_3. The thin-film structure of these organic materials, which were prepared by vacuum evaporation, produced a high brightness of green emission (from Alq_3) with a DC drive voltage of <10 V and an external quantum efficiency (EQE) of about 1% (Figure 1.1a). The injected hole and electron were shown to accumulate near the *p*–*n* heterojunction where the probability of charge recombination was greatly enhanced to produce light. It was soon discovered that the bilayer structure was not sufficient to produce all colors at will and was later evolved to a trilayer device structure with an additional thin emission layer (EML) inserted into the junction. Thenceforth, RGB emissions were enabled by the invention of the guest–host doped emitter [6], which would later to become the foundation for full-color OLED displays of today.

A typical multilayered small molecule OLED architecture is depicted in Figure 1.1b, in which an electron (EIL) and a hole injection layers (HIL) are inserted in-between the cathode/electron (ETL) and anode/hole transport (HTL) layers, respectively, to reduce charge–injection barrier and enhance carrier–charge balance for recombination in the doped EML. Subsequently, in 1990, a new kind of polymer light-emitting diode (PLED) having about 100 nm luminescent and conducting PPV thin film prepared by solution coating was discovered by Friends and coworkers at Cambridge [8]. Its substantial charge injection took place just below 14 V (corresponding to an electric field of about 2×10^6 Vcm^{-1}), and the device was able to achieve an EQE up to about 0.05%.

Organic Electroluminescence: From Molecular Structure to Device Performance, First Edition.
Edited by Qisheng Zhang and Le Zhang.

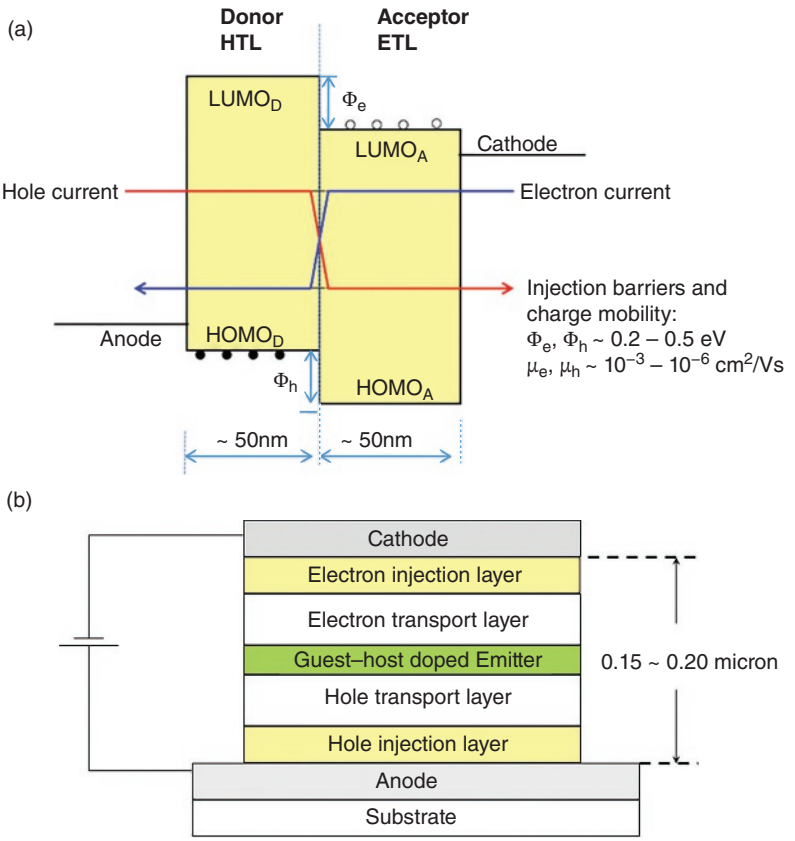

Figure 1.1 Schematic of **(a)** a typical bilayer structure. **(b)** Refined multilayer OLED. *Source:* Reproduced from [7] / permission of John Wiley & Sons.

In the ensuing three decades, tremendous R&D progress has been achieved for the improvement of OLED's charge injection, transport properties, luminance and power efficiencies, RGB color gamut, and device stability, including the understanding of its luminescence photophysics and the design/synthesis of new materials as well as optimization of device structure. Motivated by the huge potential of practical application of this new organic EL technology, the commercialization of OLED display and lighting products is well underway.

Much credit has to be given to Pioneer of Japan, which was the first Co. to recognize the potential of OLED for display applications in 1998 by introducing the first passive matrix (PM) area color display audio product for use in automobile. Thereafter, many Co's in Japan, Taiwan, and Korea followed suit in attempts to develop better materials (then mostly fluorescence), fabrication process, manufacturing equipment, encapsulation, driver electronics, array design, and module assembly for full-color PMOLEDs. But commercial success unfortunately was limited due to its line-by-line scanning pulse addressing and inefficient materials development that could only accommodate small panel size (<2″) with low resolution and brightness like those used in MP-3. Then it became obvious that for OLED to be competitive in the mainstream display market, it has to adopt active matrix (AM) addressing in order to satisfy the ever-increasing demand of

consumers for higher resolution and larger displays. The answer was quickly found in the development of low-temperature polycrystalline silicon (LTPS) thin-film transistor (TFT) backplane technology, with which, by appropriate circuit design and compensation scheme, a precise amount of micro-current can be channeled to each individual RGB sub-pixel to produce a vivid full-color display without jeopardizing its brightness, efficiency, material stability, and device lifetime. Highlights of these pioneering AMOLED CE products included the introduction of the BenQ-Siemans S88 cell phone in 2006 by AUO and the first Sony's 11″OLED TV. The timely discovery of green [9] and red phosphorescent [10] materials also aided to enhance significantly the efficiency as well as the lifetime of AMOLED, which proved to be well-suited for portable device applications. Other milestone achievements (just to name a few) at the same period of time were top-emission OLED structure to enhance RGB color gamut by micro-cavity [11]; *p–i–n* structure [12] to reduce power consumption; tandem OLED [13] to increase luminance efficiency; bipolar host [14] to reduce exciton quenching; molecular engineering to enhance blue fluorescence [15]; thermally activated delayed fluorescence (TADF) [16]; and thin-film encapsulation (TFE) [17] to protect OLED from moisture and oxygen erosion, etc., all contributed tremendously to the ultimate success of AMOLED.

Samsung of Korea is to be specially commended for developing the manufacturing-worthy side-by-side (SBS) fine metal mask (FMM) fabrication process for small-to-medium-size panels for smartphone and tablet usages, while LGD ventured into large-sized OLED TV production, adopting the maskless [WOLED + Color Filter] RGBW pixelation scheme and the Oxide TFT backplane technology. By the time, when Apple introduced the iPhone X in 2017 adopting for the first time the 5.8″AMOLED (made by Samsung with a specification of 458 ppi retinal resolution, 1 000 000:1 contrast ratio, and 625 cd m^{-2} max brightness), the establishment of OLED in the mainstream display marketplace was all but assured. Furthermore, since TOLED can be fabricated on a single crystal Si wafer with high electron mobility, OLED micro-displays with an extremely high resolution of 1920×1200 and >7000 cd m^{-2} brightness (championed by eMagin) for use as AR/VR wearable displays have also been realized in 2019. As power efficiency, out-coupling, and lifetime continue to be improved over time, white OLED will soon penetrate into the space of SSL application of indoor lighting as a unique area/surface, thin/light weight luminaire capable of delivering homogeneous, warm (most sun-like) illumination devoid of glare and blue emission hazard. It is believed that flexible display will be the "killer application" for OLED in the twenty-first century as its flexibility and freedom of form factor are unrivaled by others. Transparent OLED may also be another area of great potential to be exploited. Highlights of OLED product development in the last two decades are shown in Figure 1.2.

1.2 Characterization and Measurements

EL is the photophysical phenomenon produced by driving electrical current. A typical OLED of today comprises a multilayer structure of at least five extremely thin films (<0.2 μm in total thickness) of organic materials sandwiched in-between two electrodes on a substrate, one of which serves as the anode and the other as the cathode (Figure 1.1b). Either or both of them can be made transparent to allow electro-generated light to escape.

For introduction, its EL process can be explained by a simple working model [18] that roughly involves five steps, namely: (i) *charge injection*. As electrical bias is applied across the device, the anode is at a more positive potential than that of the cathode, and a huge electric field

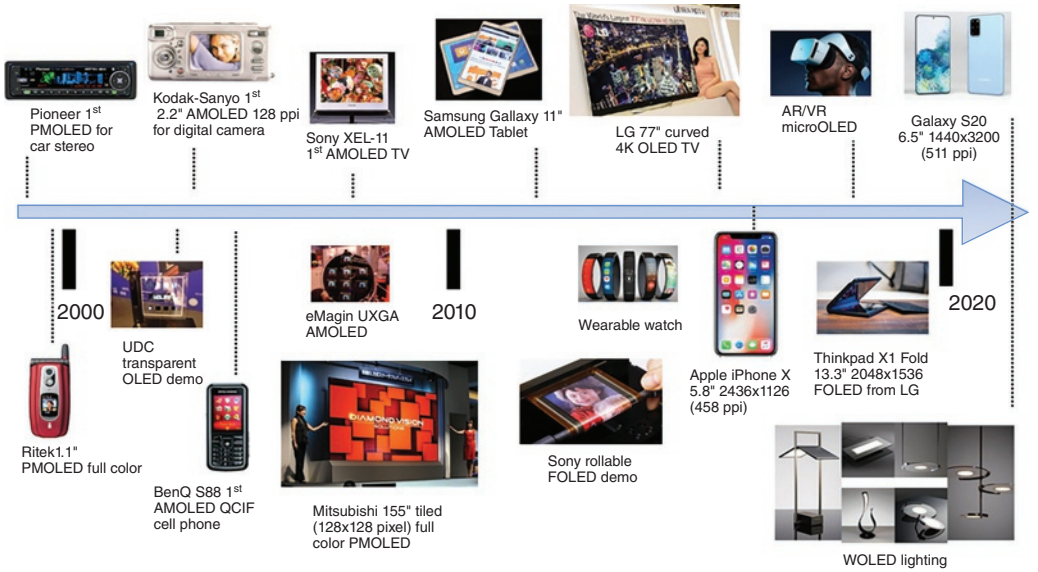

Figure 1.2 Highlights of historical development of OLED products. *Source:* Reproduced and arranged chronologically from various websites of public domain.

($>1\times10^6$ Vcm^{-1}) is generated within the entire organic layers. Injection of holes (h) occurs from the anode into the highest occupied molecular orbital (HOMO) of the HIL overcoming the energy barrier across the interface, while electrons (e) are injected from the cathode into the lowest unoccupied molecular orbital (LUMO) of the EIL; (ii) *charge transport*. Injected carriers (h and e) are transported through their respective HTL and ETL toward each other (the opposite electrodes) driven by the forward-biased potential and are confined in the EML; (iii) *exciton formation*. In the ideal case of an optimized device, the ratio of hole/electron (γ) should be one that would allow the best possibility for holes and electrons to recombine to form excitons. According to spin physics statistics (Pauli exclusion principle), for each singlet exciton (spin antisymmetrical) generated, there will be formed three triplet excitons (spin symmetrical) as well. Following spin–orbital conservation theory, only the singlet exciton can radiative relax efficiently to the ground state in the form of fluorescence, while the triplet relaxation (phosphorescence) is extremely slow (usually forbidden) without intersystem crossing (ISC); (iv) *luminescence*. Depending upon the quantum efficiency of organic photoluminescence (PL) in the EML, singlet excitons, which are short-lived, will quickly release their equivalent energy (according to their HOMO/LUMO energy gap) by decaying to the ground state in the form of light and heat; (v) *light output*. Escape of EL emission through the various layers of OLED media out of the transparent or semitransparent electrode into the air.

To characterize the EL performance of OLED, there are three basic parameters that must be considered, i.e. efficiency, color, and lifetime. In addition, the HOMO/LUMO as well as the work function and charge carrier mobility are also important parameters. The former controls the photo energy of emission (color) and the injection barrier across the metal/organic contacts between the cathode/EIL as well as that of the anode/HIL. The latter controls the transport behavior of carriers and the balance of e/h. All of them are related to the driving voltage, which ultimately impact on the power efficiency of OLED.

1.2.1 Efficiency

There are three different kinds of efficiency that characterize the EL performance of OLED, which are current (luminance) efficiency (η_{CE}) expressed in candela per ampere ($cd\,A^{-1}$), also known as nit; power (luminous) efficiency (η_{PE}) expressed in lumen per watt ($lm\,W^{-1}$); and external quantum efficiency (EQE, η_{ext}), which is the product of internal (IQE, η_{int}) and out-coupling efficiencies (η_{out}). Current efficiency is particularly useful for evaluation of OLED material performance, while power efficiency is for OLED panel design and system integration, in particular for high-resolution mobile device in which long operational time is critical. For lighting applications, light out-coupling efficiency, which dictates how much illuminating light can be extracted out of OLED, is the most important.

1.2.1.1 Current (luminance) Efficiency

In OLED, the *I-V* characteristic is most important for evaluating its foremost semiconducting property, where (I) is expressed in milliampere (mA) and current density (J) in mA/cm^2, which is a measurement of current passing through a given area ($J = I/A$), where (A) is the area of the emitter in (cm^2). Both (I) and (V) used to drive OLED can be easily determined by a voltmeter while the luminance (L) in $cd\,m^{-2}$, which is a quantitative measurement of light intensity per unit area, can be experimentally determined (L_0 is measured normal to the plane of emission) by an instrument of photoradiometer. Candela (cd) is defined as lumen (lm) per solid angle, where lumen is a photometric term of luminous flux (M), which is a measurement of quantity of light. Luminance efficiency (η_{CE}) of OLED can be calculated according to the formulation depicted in Table 1.1 [19]. It is clear that under the same driving current density, the higher the current efficiency, the more photons are produced by electron/hole recombination and vice versa.

1.2.1.2 Power Efficiency

To figure out η_{PE}, the driving voltage of OLED as well as its hemispheric luminous flux (M) expressed in lumen (lm) must be taken into account. Power efficiency (η_{PE}) expressed in $lm\,W^{-1}$ is defined as the ratio of total output of M to the total input electric power JV in watts (W) as shown in Table 1.1. When the emission of OLED is Lambertian [20] where $M = \pi L_0$, then $\eta_{PE} = \pi L_0/10JV$. For example, an OLED with an emitting area of $1\,cm^2$ driven with 5V, which produces a current of 20 mA ($J = 20\,mA\,cm^{-2}$), and a Lambertian emission with L_0 measured to be $1000\,cd\,m^{-2}$, then its current efficiency (η_L) $= 5$ cd A^{-1} and power efficiency (η_P) $= 3.14$ $lm\,W^{-1}$.

Table 1.1 EL performance parameters used in OLED characterization.

Quantity	Units	Expression
η_{CE}	cd/A	$\eta_L = L/10J$
η_{PE}	lm/W	$\eta_P = \int_0^{\pi/2} 2\pi L_0 f(\theta)\sin(\theta)\mathrm{d}\theta/JV$
η_{ext}	%	$\eta_{ext} = N_p/N_e = \int_0^{\pi/2}\int_E \frac{E_{abs}(\lambda,\theta)}{hc/\lambda}\mathrm{d}\lambda 2\pi\sin\theta\mathrm{d}\theta/\frac{I}{q}$

Definition of terms: L_0 = luminance at normal incidence [$cd\,m^{-2}$]; I = current [coulomb $C\,s^{-1}$]; J = current density [$mA\,cm^{-2}$]; V = driving voltage [V]; $f(\theta)$ = the spatial distribution of emission intensity; λ = wavelength; q = electronic charge; h = Planck's constant; c = speed of light in vacuum.

1.2.1.3 EQE of OLED

EQE is defined as the total number of output photons generated per injected electron ($\eta_{ext} = N_p/N_e$), which can be determined by using the equation depicted in Table 1.1. It is one of the most important parameters for evaluating the overall EL performance of OLED [21]. The number of electrons (N_e) can be readily calculated by $N_e = I/q$, where I is the driving current (ampere or coulomb per second, C s^{-1}) and q is the charge of an electron (1.6×10^{-19} C). But the calculation of N_p is a bit more elaborate, which requires the integration of photon energy over the entire spectrum of emission $[E_{abs}(\lambda, \theta)]$ according to the relative photopic luminous efficiency function $V(\lambda)$ divided by the photon energy ($E = hc/\lambda$) of each and every wavelength (nm) [22]. The total photon energy expressed in watts (output radiant flux W) can be measured with the aid of a photoradiometer from which the number of photons (N_p) corresponding to each wavelength of the entire emission spectrum can then be determined. Care must be taken to place the detector in the viewing direction normal to the emitter plane as close as possible and to mask waveguided and scattered light emitting from the edge and elsewhere.

In the case of measuring IQE, an integrating sphere must be employed to collect and detect all of the light that is emitted from OLED in all directions. Correction for losses inside the OLED structure must also be considered.

1.2.1.4 Out-Coupling Efficiency

In OLED, much electro-generated light can be trapped inside the bulk of the emitter due to various optical effects like waveguiding effect, internal reflection/refraction, or reabsorption by organic layers. As a Lambertian source, light escaped out of the planar cell through various layers of media with different refractive indexes (n) can be estimated by the Fresnel equation of $\eta_{out} = 1/(2n^2)$. Without means of any additional light enhancement, out-coupling efficiency (η_{out}) of a normal OLED is only about 20% for most organic media with an average $n \approx 1.5$–1.7, while ($n = 1$) for air. Thus, the external quantum efficiency (η_{EQE}) of OLED can be further elaborated by the equation of ($\eta_{EQE} = \eta_{out} \cdot \eta_{IQE}$), where η_{IQE} is the internal quantum efficiency, which is governed by the equation of ($\eta_{IQE} = \gamma \cdot \eta_r \cdot \eta_{PL}$). Here, γ is the charge–carrier balance factor (ratio of e/h), η_r is the efficiency of exciton production (spin statistic factor), and η_{PL} is the PL efficiency of the organic emissive material. Electro-generated excitons statistically have the singlet/triplet ratio of about 1/3. Abided by Pauli exclusion principle, only singlet is spin-allowed to transition radiatively to its ground state to produce fluorescence, while the spin-forbidden decay of triplet (phosphorescence) is usually too slow or inefficient to be useful (e.g. without the presence of heavy metal to promote spin–orbital coupling). Therefore, for a well charge-balanced OLED (where $\gamma = e/h = 1$), the theoretical max. of η_{INT} (with a fluorescence $\eta_{PL} = 100\%$) is limited to only about 25%, while for phosphorescence as well as TADF materials having the capability of harvesting both the triplet and singlet excitons by ISC could reach as high as $\eta_{IQE} = 100\%$.

Today, due to the high interest of developing OLED as a green and healthy indoor SSL alternative to LED, a great deal of effort has been aimed to extract more light trapped inside the OLED in order to enhance its light out-coupling efficiency (η_{out}) [23]. Detailed analysis and modeling by rigorous electromagnetic modeling of optics [24] have revealed four types of light entrapment, namely radiation mode, substrate mode, waveguide mode, and plasmon mode, as depicted in Figure 1.3a. It also shows that coupling into different modes is highly dependent on the position of the emission center, which oscillates as illustrated in Figure 1.3b. The second antinode appears to produce the highest out-coupling efficiency, while the surface plasmon mode can be minimized by fabricating the OLED emitter away from its reflective metallic electrode. To date, the most noteworthy light

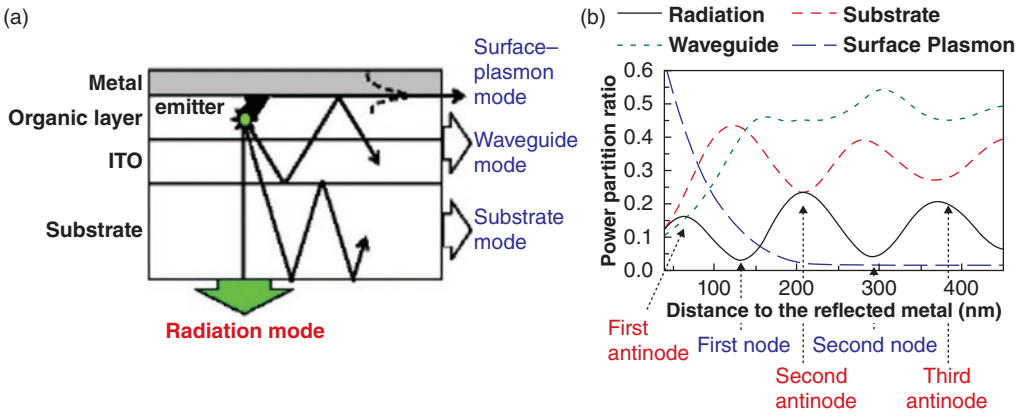

Figure 1.3 **(a)** Electromagnetic modeling of lights generated inside OLED and **(b)** their couplings with respect to the position of emission. *Source:* Reproduced from [26] / with permission of Elsevier.

extraction technology is the so-called internal enhancement layer [25], which encompasses a high-index coupling layer embedded with light-scattering particles incorporated in-between the ITO anode and the glass substrate, where η_{EQE} as high as 45% has been achieved in white OLED.

1.2.2 HOMO/LUMO and Work Function

The color of the emitted photon is corresponding to the HOMO–LUMO energy gap (E_g) of the organic luminescence material, while the energy required to overcome the injection barrier across the metal–organic contacts (anode-HIL and cathode-EIL) is related to the work functions of the metal. Both are important parameters in elucidating the EL mechanism of OLED and assessing its performance.

There are a number of methodologies by which HOMO and LUMO can be determined. Cyclic voltammetry (CV) [27] perhaps is the most common one, which is an electrochemical measurement of the relative oxidation (E_{ox}) and reduction (E_{red}) potentials against a standard electrode (e.g. ferrocene) in solution. However, since the experiment is done in solution, which invariably involves the solvation energy of the solvent molecule, it is not all that reliable, particularly for E_{red}, which is often nonreversible in the presence of air. On the other hand, the photoelectron spectroscopic measurement in air [28] as well as the UV photoelectron spectroscopy (UPS) measured in ultrahigh vacuum provides the most accurate measurement of either the ionization potential (I_p) of a thin-film solid organic sample or the work function of a metal. According to quantum mechanics, only when incident photon energy is equal to or greater than the threshold energy of the sample, can electron emission occur (and increase sharply); thence, the I_p or work function can be determined. Another method is to first estimate the HOMO–LUMO gap energy (E_g) of OLED material by way of UV-vis absorption spectroscopy to locate its long wavelength absorption onset, which should roughly correspond to the 0–0 transition between the ground (S_0) and the first excited-state (S_1) energies of the molecule. The optical bandgap (eV) energy [29] can be calculated by the equation of $[E_g = h\nu = hc/\lambda]$, where h is the Planck's constant, c is the velocity of light, and λ is the wavelength (nm). The LUMO energy (eV) can then be estimated by the difference of $[E_{LUMO} = E_{HOMO} - E_g]$.

To investigate the interfacial physics of metal–organic contact, UPS is one of the most useful instrumentations. When a metal surface or a thin-film organic material is bombarded by incident UV photons of a specific energy ($E_{uv} = hc/\lambda$) at ultrahigh vacuum ($10^{-9} \sim 10^{-10}$ torr), a photogenerated electron must overcome its binding energy (E_b) before emission can occur. By analysis of the profile of kinetic photo-electronic energy distribution with UPS, much information about electron injection across the metal–organic interface is obtained. This is because that kinetic energy (E_k) of the ejected photoelectron is equal to the incident UV energy minus the binding energy of the metal ($E_k = h\nu - E_b$). Since electron near the top of valance band of the metal has the least binding energy to overcome, the energy where the maximum kinetic energy of photoelectron is detected must be the Fermi level (Φ_m), where $\left[\Phi_m = h\nu - E_k^{max}{}_{(metal)}\right]$. Likewise, the HOMO energy level of organic material where $\left[E_{HOMO} = h\nu - E_k^{max}{}_{(org)}\right]$ can also be determined. From the difference between their maximum kinetic energies, the injection barrier (ε_v^F) across the metal–organic interface can then be estimated $\left[\varepsilon_v^F = E_k^{max}{}_{(metal)} - E_k^{max}{}_{(org)}\right]$ as illustrated in Figure 1.4.

It is to be noted that a significant shift of energy in vacuum level (E_{vac}) may result from the dipole induced by the driving voltage between the metal surface and organic contact. The amount of this shift (Δ) can be deduced by the difference in their respective minimum kinetic energies according to equation $\left[\Delta = E_k^{min}{}_{(org)} - E_k^{min}{}_{(metal)}\right]$. Hence, the LUMO of organic material can also be determined by the difference of E_{HOMO} and its optical gap energy (E_g) described before. There is a lesser common but more sophisticated instrumentation like inverse photoemission spectroscopy [30], which allows LUMO of organic materials to be measured directly. Besides, there are also a couple of theoretical models based on semiconductor physics, injection limited [31], and space charge limited [32] to predict and explain the injection current better in which readers may be interested.

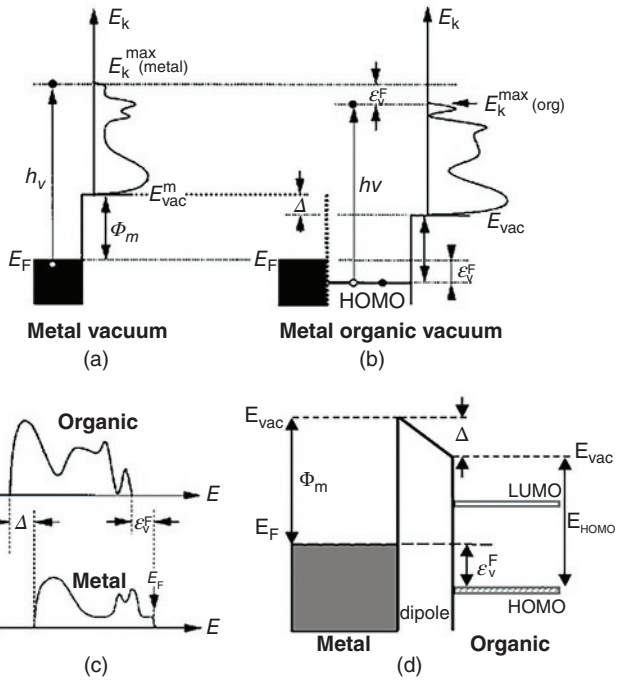

Figure 1.4 **(a)** Carrier–injection barrier determined using UPS and **(b)** its energy diagram **(c)** profile of kinetic photo-electronic energy distribution and **(d)** interfacial energy diagrams of metal electrode/organics.

1.2.3 Carrier Mobility in Organic Materials

Mobility (μ) is another important parameter in the characterization of OLED, which impacts on the carrier balance (γ), driving voltage, and eventually its power efficiency. It is a good indicator to show how efficient (or how fast) injected charge carriers can move under a specific electric field. Once e and h are injected into the organic layers, they must be transported toward each other through their respective ETL and HTL to recombine in the EML. But, unlike inorganic semiconductors, thin-film organic materials are amorphous in nature, and they fail to have a continuous conduction band in which to move electron freely. Transporting e and h between neighboring organic molecules has often been rationalized by a hopping mechanism [34], which involves their relatively free delocalized π-electrons in LUMO and HOMO, respectively.

There are many methods [35] by which the mobility of organic materials can be determined, such as space charge limited current and time of flight [36] (TOF), transient EL [37], OFET, and admittance spectroscopy [38]. By far, the most widely employed is that of TOF, particularly for hole mobility measurement according to the setup illustrated in Figure 1.5 [39], in which a nitrogen pulse laser at 337.1 nm is used as the excitation source. A rather thick layer of testing sample (5–10 μm) is prepared by vacuum evaporation between two electrodes, one of which is transparent (ITO) and the other is semitransparent like Al. To facilitate photogeneration of charge carriers, a thin charge generation layer (CGL) is often inserted in-between the electrodes as in [ITO/sample/CGL/Al]. For hole mobility measurement, the laser beam is incident from the semitransparent Al side, and the photogenerated holes are collected at the ITO electrode. For electron mobility, the laser is incident from the ITO side. A DC power supply was used to provide the necessary bias voltage to the sample for the relevant carrier detection. The resulting electric field across the sample is usually maintained in the range of 10–1500 kV/cm.

The mobility μ expressed in ($cm^2V^{-1}sec^{-1}$) is computed using the well-known relation of [$\mu = d^2/(V \cdot \tau)$], where V is the applied voltage, d is the sample thickness, and τ is the flight time in μs as determined from the plot depicted in Figure 1.5. During the measurement, care must be taken to ensure that the thick layer of tested sample does not crystallize. In general, the mobility of organic electron transport material (ETM) is orders of magnitude slower than that of hole transport material (HTM). Besides, ETM is also more difficult to measure as it is extremely sensitive to ambient air/oxygen, which can serve as an extrinsic dopant to induce carrier trapping in the sample.

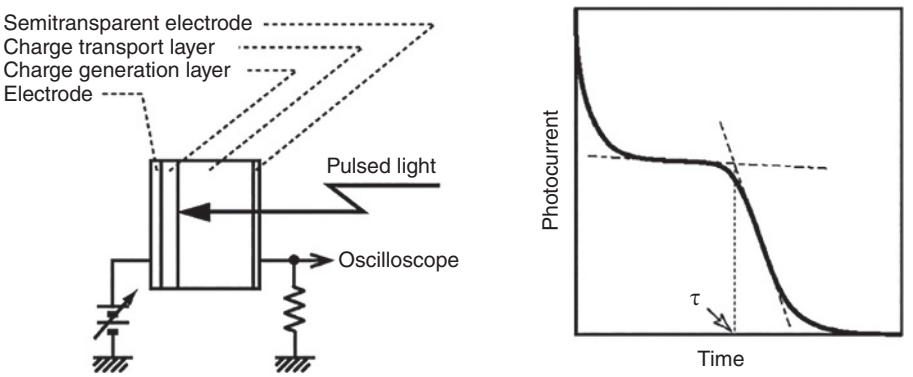

Figure 1.5 Carrier mobility measurement by TOF. *Source:* Reproduced from [40] / with permission of American Chemical Society.

1.2.4 Color

1.2.4.1 Absorption and Emission Spectra

One of the ways to characterize OLED color is by first examining the thin-film PL of its emissive material, which, without any optical effect, should bear considerable resemblance to that of its EL. This is because the radiative decay pathway of electro-generated excitons in the excited states is similar to that of the PL relaxation. To understand the origin of emissive color, some basic knowledge about photo-excited absorption and emission can be very useful. A fundamental photo-excited absorption and emission relationship in a potential energy diagram is illustrated in Figure 1.6. According to Franck–Condon principle, the energy of emission bands is always lower than that of the absorption, and they are essentially mirror-symmetric and overlap with each other at the shorter wavelength region. The displacement of luminescence maximum toward longer wavelengths than that of the absorption maximum is known as the Stokes shift, which often indicates the nonradiative losses involved in luminescence [40]. The extent of Stokes shift also reveals information related to change of molecular geometry in the excited states, with rigid molecule having much smaller shift than that of flexible. As can be seen in Figure 1.6, the 0–0 energy transition should represent the optical bandgap energy (E_g) of the emissive material, which is equal to its HOMO–LUMO gap energy as described previously in Section 1.2.2.

Another important parameter that can be extracted from photo spectroscopy is that of the excited-state lifetime, which can be measured by time-resolved spectroscopic technique. A typical trace of this transient PL spectrum is depicted in Figure 1.6, in which the average lifetime (τ) of the excited state can be determined using the equation: $[I = I_0 e^{-t/\tau}]$, where I and I_0 represent the transient and initial PL intensities, respectively, and t is the time of PL decay measured in μs. Excited lifetime of fluorescence is usually very short (in nanoseconds), while that of phosphorescence can be as long as milliseconds (even seconds) without any spin–orbital coupling. Many luminescence

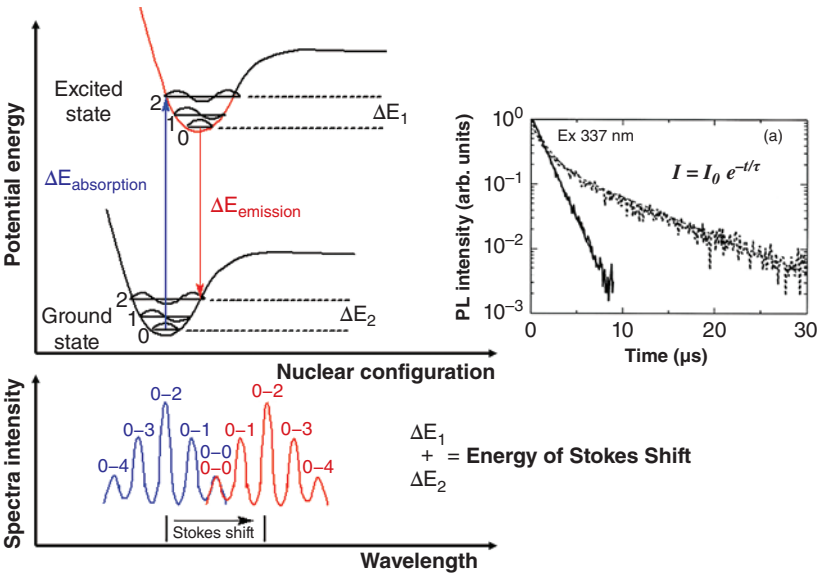

Figure 1.6 Potential energy diagram of Franck–Condon principle and example of transient PL.
Source: Adapted from Prof. Chin-Ti Chen.

materials have considerable delayed fluorescence, which can be harvested to boost quantum efficiency either by triplet–triplet annihilation (TTA) or by molecular engineering like that of TADF molecule.

1.2.4.2 CIE Chromaticity Diagram

In order to evaluate whether organic emissive material is device worthy in OLED as an emitter, early investigation about its PL wavelength λ_{max} (nm), relative quantum efficiency, and full width at half maximum (FWHM) can be very informative. But for display application, a more precise and elaborate system of measurement of color must be considered.

Color (chromaticity) specification and measurements with their bewildering terminology and concepts of photometry, radiometry, and spectrophotometry can be a formidable subject for many who happen to not expertise in colorimetry. Luckily, with the help of modern instrumentation like colorimeter, spectrophotometer, and spectroradiometer, much of the difficult task of algorism is alleviated. In emissive displays like OLED, colors are additive, whose three primaries are red (R), green (G), and blue (B). When RGB are emitting in the proper ratio, white (W) light is produced and contrarily, a true black is produced, when all are off. Intermediate combinations of RGB result in the capability of producing all colors and shades.

The 1931 $CIE_{x,y}$ Chromaticity System [41], commonly used in OLED characterization, was devised by the Commission Internationale de l'Eclairage, which is an international organization devoted to the specification of light and color. The CIE chromaticity diagram shown in Figure 1.7 allows any color viewable by the average human eye to be specified by a pair of coordinates, x and y, which are derived from the CIE tri-stimulus function involving the tri-stimulus value of X, Y, and Z. These are three carefully prescribed spectral sensitivity curves (as shown in the bottom of Figure 1.7a) [42] that stimulate the sensitivity of the average human eye receptors to R, G, and B,

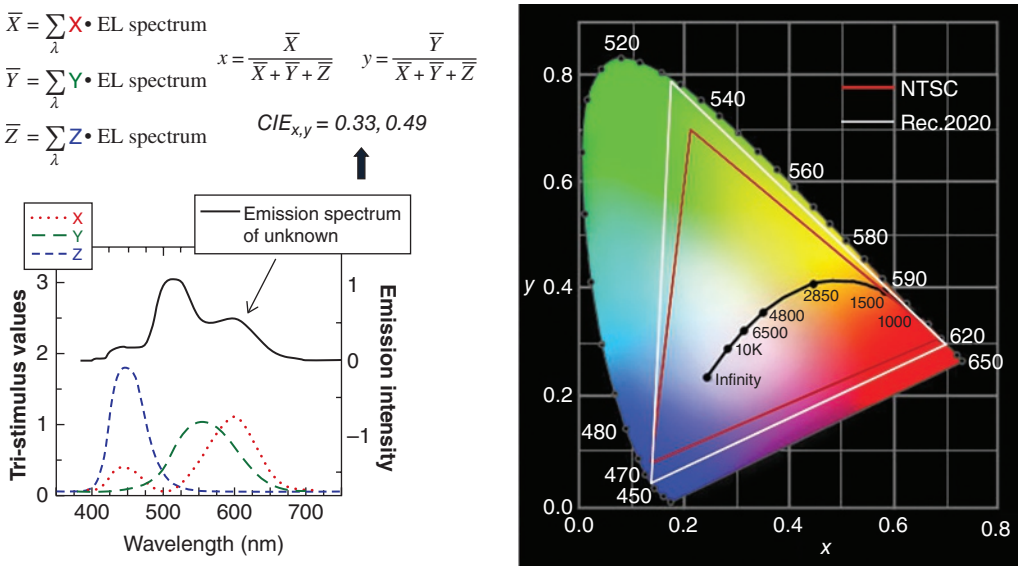

Figure 1.7 **(a)** Tri-stimulus *X, Y,* and *Z* spectral sensitivity curve and **(b)** 1931 $CIE_{x,y}$ chromaticity diagram. *Source:* Reproduced with permission Prof. Stephen R. Forrest.

respectively. The $CIE_{x,y}$ of each and every λ (nm) of the EL spectrum can then be determined by X and Y divided by the summation of X, Y, and Z, respectively, where $[x_{(\lambda)} = X/(X + Y + Z)]$ and $[y_{(\lambda)} = Y/(X + Y + Z)]$. The algorithm involved is illustrated by an example of OLED's EL spectrum depicted as the upper curve in black in Figure 1.7a. It is apparent that the CIE chromaticity diagram is able to assign simple *x,y* coordinates in a user-friendly way to any EL spectrum in question and thus describe the color precisely. For instance, the $CIE_{x,y}$ system is possible to predict the resulting color by combining any two colors. If two emissive colors are represented by two points on the diagram, the result of adding them will always be on the line joining the two points. The area bounded by the horseshoe-shaped perimeter defines the limits of the colors and is termed the color space. Color saturation or purity increases as it approaches the outer periphery of the chart and shifts to neutral white as the center is approached.

As shown in Figure 1.7b (brown line), the respective location of the three primary RGB colors defined by the NTSC (National Television System Committee) constitutes a triangular area on the 1931 $CIE_{x,y}$ color chromaticity diagram, which is also called color gamut. Color saturation is defined as the ratio of color gamut area of a display relative to that of the NTSC standard. For AMOLED, color saturation can well exceed 100%, particularly in a top-emission device with a micro-cavity structure as to be described later. Recently, due to the advent of ultrahigh definition (UHD) of 8K TV, the old NTSC is no longer adequate in defining the color space of future displays [43]. A new system of parameters of *Rec. 2020* is therefore adopted, which is short for "*Recommendation ITU-RBT.2020-2, Parameter values for ultra-high definition television systems for production and international programme exchange.*" Its new specifications [44] in terms of $CIE_{x,y}$ color chromaticity are R (0.708, 0.292), G (0.170, 0.797), B (0.131, 0.046), and a reference (D65) White of (0.3127, 0.3290) as illustrated in Figure 1.7b (represented by the white triangle).

For OLED lighting application, the color appearance or correlated color temperature, which describes the extent of whiteness of a white light source, is important. A cool white temperature is over 6500 K (D65), and a warm white temperature is less than 3000 K. When the heated black body showing a same or nearly same extent of whiteness as the testing white light source, the temperature determined from the heated black body is the color temperature of the white light source. Color rendering index (CRI) is another physical term for comparing the color contrast of an object illuminated by the sun to that obtained by the testing illuminator. For instance, WOLED needs to reach at least CRI >80 in order to be considered practical for SSL application. CRI of sun illumination is defined as 100, which is the best possible value for any illuminator.

1.2.5 Operational Lifetime

No OLED is useful unless it is "stable," and that is why operational lifetime (or lifetime) is considered as one of the most critical parameters in OLED characterization. The lifetime of OLED is defined as the time needed for luminance to drop to a specific level, for instance, to 50% (LT50 or $t_{1/2}$), 70% (LT70), or 90% (LT90) of its initial value driven at constant driving current. To measure the lifetime within a reasonable timeframe, it is often necessary to accelerate the test procedure. Stretched exponential decay (SED) [45] is a very effective and widely accepted methodology to obtain lifetime data in the OLED community. It can be expressed by the equation: $L = L_0 \, exp[-(t/\tau)^{\beta}]$, where L_0 is the initial luminance (cd/m^2), t is the time parameter (h), L is the luminance measured at a given time, β is a constant form factor of SED, and τ is the coefficient related to L_0, which depends on accelerated condition. Since the rate of luminance decay is proportional to the initial luminance (L_0), the value of scale factor τ can be extracted by the decay lifetime of

OLED driven at various L_0. For instance, from the linear relationship of plots of $t_{1/2}$ versus (various) L_0, LT50 can be readily estimated with any initial luminance using the expression: L_0^n $t_{1/2} = \text{const}$.

The SED function has been shown to be valid for predicting the accelerated lifetime of a wide variety of OLEDs, including the single-colored fluorescence and phosphorescence multilayer devices [46], provided that: (i) the short-term luminous degradation portion (which is usually very small) can be ignored for curve fitting; and (ii) the sub-exponential component remains constant even when the accelerated testing conditions are varied. It should be noted that under high current drive conditions, considerable heat can be generated in the OLED panel, which may impact on the analysis by simple SED extrapolation. Recently, an improved method of lifetime prediction [47] that decouples Joule self-heating effect from coulombic degradation in accelerated aging test of OLED has been proposed. This approach takes into account of the real temperature (measured) of the test OLED sample (T_{EL}), current density (J), and the primary long-term decay time (τ), whose relationship is expressed by the equation: $1/\tau = AJ^{\beta} exp(-E_a/kT_{ET})$, where A is a constant, k is the Boltzmann constant, and E_a is the activation energy derived from the slope of the Arrhenius plot of inversed τ versus T_{EL} for various J as a parameter. Thus, using the activation energy (E_a), the effect of temperature on the device degradation lifetime can be corrected.

1.3 OLED Materials

EL performance of OLED depends very much on the materials used in the device. Therefore, it is not surprising to hear often in the trade: "Good material makes good device!" Since a comprehensive coverage of OLED materials is beyond the scope of this chapter, only certain components that are essential to the making of OLED, such as substrates, electrodes, organic functional, capping (passivation), and encapsulation layers, are discussed in this section.

1.3.1 Substrates

Glass is widely considered as the best substrate for both the front- and backplanes (LTPS-TFT) of OLED fabrication due to its cost advantage (abundantly available), long lifetime, low coefficient of thermal expansion (CTE ~3 ppm K^{-1} for non-alkali borosilicate glass) and surface roughness (Ra <0.3 nm), high optical transmittance, and excellent chemical resistance (for wet processing), heat resistance (T_g >900 °C), and water vapor and oxygen non-permeability. The only problems appear to lie in its ease of breakage (brittle) and rigid form factor, which greatly limit glass to meet the future demand and requirement of flexible displays. To date, the most studied flexible substrates for FOLED are ultrathin glass (UTG) [48], stainless steel foil (SSF), and plastic films.

1.3.1.1 Ultrathin Glass

UTG refers to a type of high-quality flexible glass whose thickness is reduced to less than 100 μm. It is able to retain all the excellent attributes of regular glass substrate except for one major drawback – that is its increased shock sensitivity and handling difficulty. By protective overcoating and laser-cut edges, much progress has been made to improve its mechanical strength and reliability and thus enable both sheet-to-sheet and roll-to-roll (R2R) device fabrications [49].

UTG has been shown to be compatible with high processing temperature (>400 °C) from which high-quality ITO film with resistivity of $1.7 \times 10^{-4}\,\Omega$cm and transmission of >84% have been

achieved [50]. Recently, Samsung also decided to use UTG as a protective cover for its newly released foldable smartphone: Galaxy Z Fold 2.

1.3.1.2 Stainless Steel Foil

SSF [51] has been considered as a viable substrate for flexible displays because it is mechanically durable, shock resistant, thermally and chemically stable, and also has excellent barrier property. But due to its intrinsic conductivity, opaqueness, and very rough surface, SSF has not found much success in FOLED application despite much effort in overcoating it with insulating film and surface planarization.

Recently, it was reported that planarized SSF [52] could be employed as a reflective electrode for OLED lighting using R2R sputtering, screen printing, and wet-cleaning equipment. The electrode, which was composed of Ag alloy (100 nm) and ITO (15 nm), was prepared and patterned by screen printing with etching paste followed by heat treatment and washing.

1.3.1.3 Plastic Films

It covers a large number of commercially available synthetic films that could be used as FOLED substrates, which include, in particular, polyethyleneterephthalate (PET), polyethylenenaphthalate (PEN), and polyimide (PI), whose material properties are compared with those of SSF and UTG in Table 1.2.

It is clear that nearly all plastic films have a high water vapor transmission rate (WVTR) and a large CTE, which are common issues of polymeric material. While PET is known for its superb quality of optical transmission and cost advantage, it is useless as a substrate owing to its extremely low T_g. PEN [53] is considered a borderline candidate as its T_g is still well below the mildest processing window of oxide TFT backplane even though upper processing temperature of 200 °C has been claimed. This leaves PI with its exceptionally high thermal endurance and relatively low CTE the de facto choice of substrate for FOLED. Some PI (T_{dec} > 560 °C) has been reported [54] to be able to withstand processing temperature up to 450 °C, which is essential for LTPS-TFT backplane fabrication – a thoroughbred for small-to-medium-sized high-resolution OLED products. But unfortunately all high T_g-PI are yellowish (amber color) which absorbs considerable portion of blue emission, thus renders it unsuitable for bottom-emission device.

Lured by the tremendous market demands and reward of investment, there is a great deal of R&D efforts trying to develop high T_g colorless PI films (cPI). On the molecular level, this is

Table 1.2 Comparison of material properties of flexible substrates.

Plastic Substrate	Tg (°C)	CTM (ppm/°C)	Thickness (μm)	Transmittance (%@ 550 nm)	WVTR ($gm^{-2}d$, @ rt)	Bend Radius (mm)	Dimension stability	Cost
SSF	1400	14–16	20–100	—	~0	63	Excellent	High
UTG	600	3–8	50–100	93	~0	35	Excellent	Very high
Yellowish PI	400 –490	10–20	20–125	—	0.4–10	~5	Very good	medium
Colorless PI	300 –400	10–20	25–55	<90	0.4–20	~5	Good	High
PEN	180	18–20	50–125	87	7.3	<5	Good	Low
PET	78	15	125	>91	3.9–17	<5	Poor	Very low

accomplished by the incorporation of fluorine or bulky (steric) substituents in the copolymer to enlarge the HOMO–LUMO bandgap energy of PI, thus to shift its inherent absorption from blue to UV. But, so far, it has been challenging as nearly all cPI produced [55] invariably have considerably lower T_g (<400 °C), which could barely meet the processing conditions of IGZO-TFT backplane fabrication of today. Instead, most of the commercially available cPIs are employed as flexible cover sheets and touch panels of OLED with great success. Recently, however, it was reported [56] that a new transparent PI varnish after curing under nitrogen at 360 °C can produce PI film with a T_g as high as 459 °C, 88% transmission, 0.3% haze, and a low CTE of 13.7 ppm K^{-1}.

In order to meet the stringent requirement of FOLED to exclude moisture and oxygen from penetration, the WVTR of PI must be further reduced by passivation [57], for instance with SiN_x-SiO_x using plasma-enhanced chemical deposition (PECVD) at temperature below 300 °C. A typical process flow always involves a carrier glass to provide rigid support for PI during the precision fabrication protocol before de-bonding in the end by laser lift-off. PI film can be formed by casting its precursor polyamic acid varnish on glass support followed by imidization by thermal or chemical treatment. Bonding and de-bonding of PI film from carrier glass can be tricky in manufacturing, as it can ultimately impact on amorphous IGZO-TFT's performance [58].

1.3.2 Anode and Cathode Electrodes

It is important that the work functions of anode and cathode electrodes of OLED be compatible with the HOMO of the adjacent HIL and LUMO of EIL, respectively. This is to minimize the injection energy barriers existing between electrode/organic contacts that may impact on device driving voltage and power consumption.

To ensure that hole can effectively be injected from the anode to the HOMO of the appropriate hole injection materials (HIMs), semiconducting transparent conductive oxides (TCOs) with high work function are preferred. ITO (indium tin oxide) is the most useful anode for OLED, which exhibits high electrical conductivities (1×10^{-3}–$1 \times 10^{-5}\,\Omega$ cm), high work function (4.5–4.8 eV), and outstanding optical transparencies (~90%) in a broad visible spectral region to allow light output from the device. Its sheet resistance, which is highly dependent upon the sputtering conditions, is inversely proportional to processing temperature as well as the thickness of deposited ITO (albeit at the expense of roughness). In order to further reduce the barrier of hole injection, oxygen plasma or UV ozone [59] pretreatment has been necessitated to enhance the hole injection properties of ITO.

Due to the recent surge of flexible OLED applications, IZO (indium zinc oxide) has been widely investigated as an alternative to ITO, which often needs high substrate or post annealing temperature (above 200 °C) that proves to be not compatible with many low T_g flexible plastic substrates. It has been shown that high-quality IZO film can be prepared at a much lower substrate temperature (<100 °C) by using a radiofrequency (RF) magnetron sputtering system equipped with an ion gun (ion-beam treatment of substrate prior to sputtering deposition) [60]. In a comparative study, the best sheet resistance of IZO films thus obtained was measured to be 25 Ω/□ for glass and 20 Ω/□ for PET substrates with a thickness of 150 nm while their lowest root-mean-square (rms) roughness remains only at 0.58 and 0.32 nm, respectively. It was demonstrated that both ITO and IZO can be deposited on UTG and post annealed with the dynamic flash lamp technique [50] to achieve similar results of high-quality films with low sheet resistance without the detrimental effect of furnace heating. The main advantage of ultrafast thermal annealing technology is that only the surface heats up while the bulk flexible substrate remains cold to avoid deformation. For lighting

application, AgNWs (silver nanowires) imbedded in polyvinyl butyrate [61] have been demonstrated as a potential anode in FOLED, which achieved a sheet resistance of 25 Ω/□ with a transmittance of 92% in the visible spectrum. There were also reports to use graphene [62, 63] as a transparent conductive anode, but its commercial success is greatly hampered by the difficulty in processing, scaling, and cost of production.

For top-emitting OLED (TOLED), the anode needs to be highly reflective to create the optimal micro-cavity for color gamut enhancement. This is best accomplished by overcoating a thick layer of reflective Ag (~150 nm) on a thin layer of ITO (10 nm) on a glass substrate, which is capable of achieving over 90% reflectance in the visible wavelength region [64]. Likewise, to ensure that an electron can effectively be injected from the cathode to the LUMO of the appropriate electron injection materials (EIMs), metal with low work function must be considered [65]. The most commonly employed metal or metal alloys are Li, LiF/Al [66, 67], and Mg:Ag, with work functions of about 2.95, 2.50, and 3.70 eV, respectively.

In TOLED, a semitransparent top cathode plays an important role for controlling the micro-cavity and achieving good device performance. Thin layers (10–20 nm) of metal like Mg:Ag and Al/Ag are two of the widely employed compositions. Recently, it has been shown that the composition of Mg:Ag (1:10) appears to be better than that of (10:1), and in addition, low-absorption, thin (20 nm) pristine Ag coupled with proper *n*-doping is also very good for TOLED micro-cavity device [68]. To decrease the reflection of ambient light from the semitransparent cathode and increase contrast, Ag:WO_3 [69], which is made of silver nanocrystals with diameters around 5 nm embedded in amorphous WO_3, has also been demonstrated in TOLED.

1.3.3 Hole Injection and Transport Materials

To reduce the drive voltage of OLED, it is important that holes can be readily injected from the anode with high work function (e.g. ITO) while the electron from the cathode with low work function (such as Li, Ca, Mg, Mg:Ag, Al) with ease. On the other hand, organic-layered stack must also be thin in order to create sufficient electric field (~10^6 V cm^{-1}) to transport charges, as nearly all organic materials are basically insulating. It's been established by many detailed studies [70] that the largest voltage drop in driving OLED is caused by the large energy barrier (Φ_h, Φ_e about 0.2–0.5 eV) that exists between the HOMO of the HTL and the work function of ITO as well as the LUMO of the ETL and the work function of the metallic cathode. It was subsequently found that this energy barrier can be mitigated greatly by inserting a HIL with a proper HOMO energy level lying in-between those of the anode and HTL as well as an EIL with a proper LUMO in-between those of the ETL and the cathode. Thus, most robust small-molecule OLEDs of today with the best EL efficiency are found to contain multilayered organic stacks as depicted previously in Figure 1.1b.

In the development of OLED HIM and HTM, many functional molecules have been designed and synthesized for the purpose of enhancing hole injection and mobility. Nearly all of them are excellent donor molecules containing several highly electronegative "nitrogens" that are regiospecifically positioned to raise the HOMO level of HIM (e.g. MTDADA [71] is about −5.2 eV while NPB is −5.6 eV) to match the work function of ITO (raised from −4.7 eV to about −5.2 eV after UV-ozone pretreatment). The addition of a *p*-type dopant to an appropriate organic transport material has been shown to be extremely effective in eliminating the interfacial injection barrier between the ITO and HIL (ohmic contact) [72]. As a result, further reduction of drive voltage in AMOLEDs can be realized. There are many inorganic *p*-dopants that have been proven effective, like WO_3 [73], MoO_3 [74], and $FeCl_3$ [75]. The most widely employed *p*-dopants are F4-TCNQ [76],

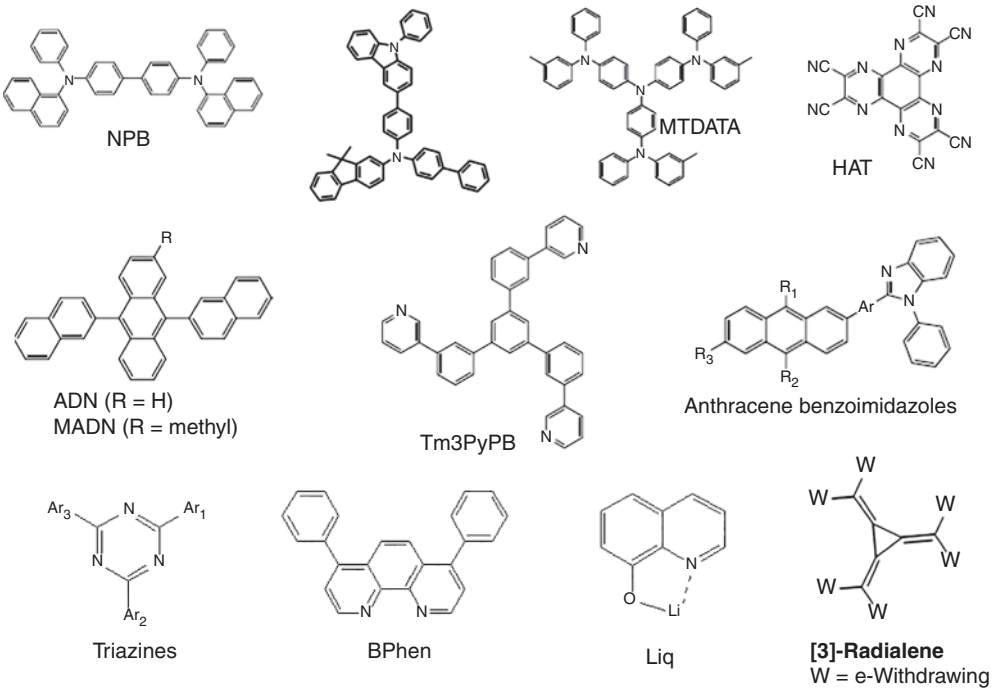

Figure 1.8 Examples of HTM and ETM with typical *p*- and *n*-dopants.

HATCN [77], and [3]-radialenes [78], which are all excellent organic electron-withdrawing acceptors with an extremely low LUMO (about −5.2eV or lower) capable of oxidizing most of the HIMs by electron transfer. For HTMs, it is also important that they possess thermal stability with high glass-transition temperature (T_g), high-hole mobility, and the capability of forming stable pinhole-free thin films upon evaporation. Some of the commonly employed HTMs are biphenyl diamine derivatives [79] (e.g. NPB); starburst amorphous molecules [80]; and spiro-linked biphenyl diamines [81]. There is also an interesting family of aromatic derivatives based on the anthracene molecule that exhibits not only bipolar characteristics but also ambipolar [82, 83] having similar hole and electron transport mobility ($\mu_h \sim \mu_e$). These HTMs have been shown to improve the lifetime of OLED. Representatives of HIM and HTMs with *p*-dopants are shown in Figure 1.8.

1.3.4 Electron Injection and Transport Materials

For organic materials, usually the charge transport property of electron is much inferior to that of hole. Therefore, in order to maximize the probability of charge balance for recombination in the EML, it is very important to facilitate the electron injection from the cathode. Typical EIMs are LiF [84], CsF [85], and Liq [86, 87] or nonmetal *n*-type dopants [88] that are capable of lowering or even eliminating the energy barrier existing between the cathode and the EIL in the *p*–*i*–*n* devices. Today the most widely used EIM found in many OLED products still appears to be the old workhorse, Liq and LiF (in contact with Al cathode), even though there are reports that evaporated Li metal (which may contain traces of Li_2O) in the presence of BPhen as ETM [89] works just as well in WOLEDs. For TOLED, an ultrathin layer of ytterbium (Yb) has also been found to be effective as an electron injector [90].

Good ETMs, besides the usual high T_g thermal property, should also have high electron-transport mobility (μe) and preferably hole-blocking capability. Some of the best examples are pyridine based Tm3PyPB [91], phenanthroline-based BPhen and BCP [92], anthracene–benzimidazoles [93, 94], and triazine-based ETM (TAZ) [95] (Figure 1.8). Recently, it has been shown that if the Ar_{1-3} substituents in TAZ structure contain metal-coordination sites (e.g. pyridine), they can also exhibit excellent electron injection characteristics for transparent OLEDs [96].

1.3.5 Luminescent Materials

A good many reviews [97, 98] have been written on the subject of luminescent RGB materials, which are considered one of the most important elements in OLED. To date, the most efficient and robust technology of color generation is still based on the guest–host system [6] despite many attempts trying to make nondopant emitter in OLED. By all things considered (efficiency, color, and lifetime), the best working set of luminescent materials is none other than one of the hybrids in which red and green emitters are phosphorescence while that of blue remains to be fluorescence. There have been decades of endeavors throughout the world aiming to develop a true blue phosphorescent molecule (CIEy < 0.15) with sufficient efficiency (without roll-off) and long lifetime but unfortunately remaining fruitless to date. Although the new TADF material is promising and emerging, it would be quite a while before turning into a serious contender in the marketplace. Here, we highlight only the developments of certain commercially significant materials while leaving most of the in-depth discussions on photophysics and chemistry of luminescence to the expert authors in the ensuing chapters.

The development of luminescent materials can be summarized [26] over the last 40 years in roughly four stages as depicted in Figure 1.9. Gen.1 characterizes early OLED materials development (beginning in the 80s in Kodak [99]), which has all been focused on the design and synthesis of fluorescent molecules that can only harvest singlet excitons. Gen. 2 began with the discovery of phosphorescent molecules [100, 101] in the 90s that can harvest both the singlet and triplet excitons by incorporating heavy metal (mostly iridium and platinum) into the luminescent molecular complex. Utilizing the heavy atom effect that promotes spin–orbital coupling, these second-generation luminescent materials all possess a hybrid emissive excited state of singlet and triplet excitons with very short excited state lifetime (in μs) thus easing up the forbiddance of room temperature phosphorescence. Gen. 3 started in 2012 with the discovery of certain (TADF) molecules [102, 103] possessing very small singlet–triplet energy gap (ΔE_{S-T}), which allows efficient reversed intersystem crossing (RISC) and delayed fluorescence to emit with $IQE_{max} \sim 100\%$. Shortly after, it was discovered that some TADF molecules can also function as hosts to transfer all of their harvested singlet and triplet exciton energy to the appropriate RGB guest molecules to fluoresce by Förster resonance energy transfer. The resulting emission is called hyperfluorescence [104], which is capable of producing improved $CIE_{x,y}$ color purity with a maximum IQE of 100%, and this type of luminescence material is amicably designated as Gen. 3.5.

Finally, it must be mentioned that there was also reported a special class of luminescent materials [105] (e.g. TPA-NZP) that could harvest triplet excitons efficiently without possessing the very small singlet–triplet energy gap (ΔE_{S-T}) as that of the normal TADF. The novel RISC mechanism was rationalized by detailed modeling and supported by experiments to involve a hybridized local and charge transfer excited state through the hot exciton CT manifold of $T_2 \rightarrow S_2$. Unfortunately, so far few molecules in this class have been reported to further substantiate this claim nor has the hot exciton mode of triplet harvesting been widely investigated independently. Otherwise this special class of molecules could very well be called the fourth generation of luminescent materials discovery [106, 107].

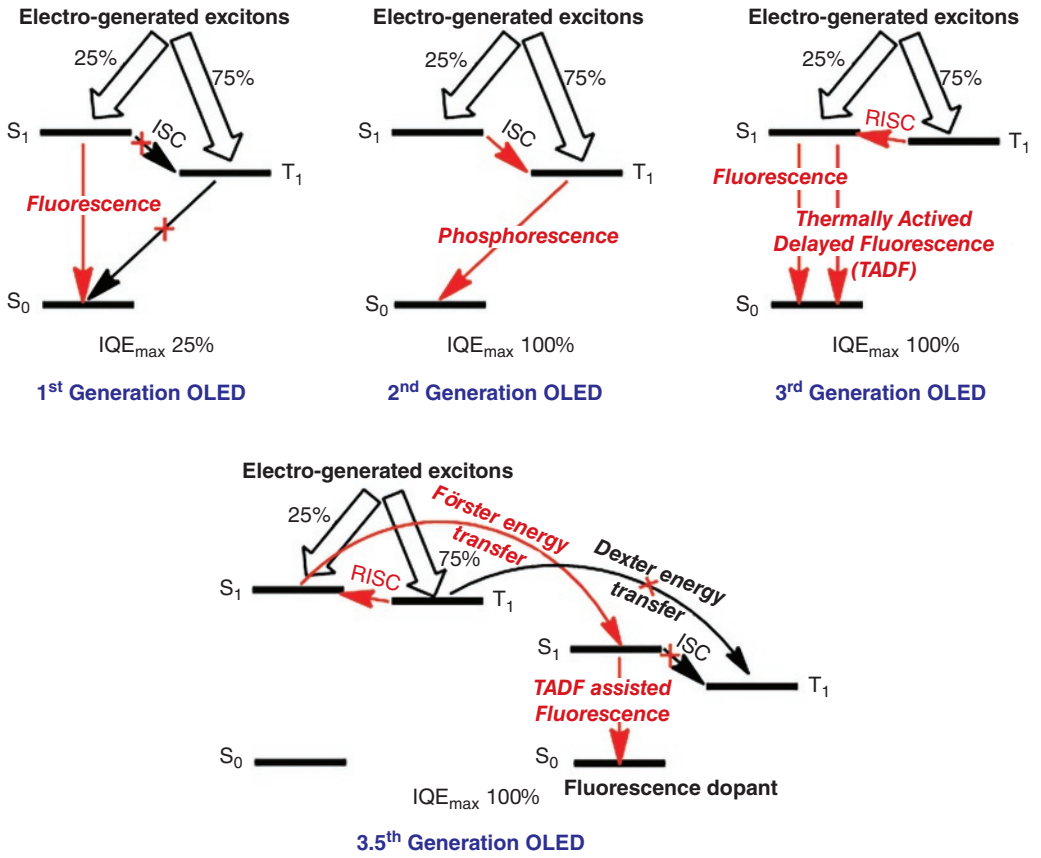

Figure 1.9 Evolution of luminescent materials of OLED. *Source:* Reproduced from [26] / with permission of Elsevier.

1.3.5.1 Host Matrix System

In an ideal guest–host emitter system in OLED, host material plays a critical role in controlling carrier balance as well as the efficiency of energy transfer (to an energy-compatible dopant), which ultimately impacts on lifetime as well. One of the serious issues in electrophosphorescence is that its efficiency tends to roll-off at high luminance, which has been shown to be primarily due to TTA occurring at high triplet concentration. One of the best solutions is to mix both HTM and ETM [14, 82, 83] in the host matrix to affect efficient host–guest energy transfer. Using two hosts with different transporting properties also facilitates carrier balance adjustment in the EML. It has also been reported that the proper choice of *n*- and *p*-type hosts induces the formation of exciplex, which promotes exciplex-triplet energy transfer (ExTET) in enhancing the efficiency and lifetime [108]. To prevent triplet exciton from quenching, a substituent of sufficiently high triplet energy (like dibenzothiophene or dibenzofuran) may also be incorporated into the host molecule. Recently, it was found that by premixing both host materials prior to doping in a vacuum can be very beneficial as it not only simplifies thermal evaporation protocol (reduced from 3 evaporation sources to 2) but also aids to enhance the performance of OLED [109].

Next came the specially designed bipolar host molecules in which both hole- and electron-transporting moieties of graded electronegativities are strategically engineered into the molecule by a linking group [L], such as 2-phenyl-4,6-bis(12-phenylindolo[2,3-a] carbazole-11-yl)-1,

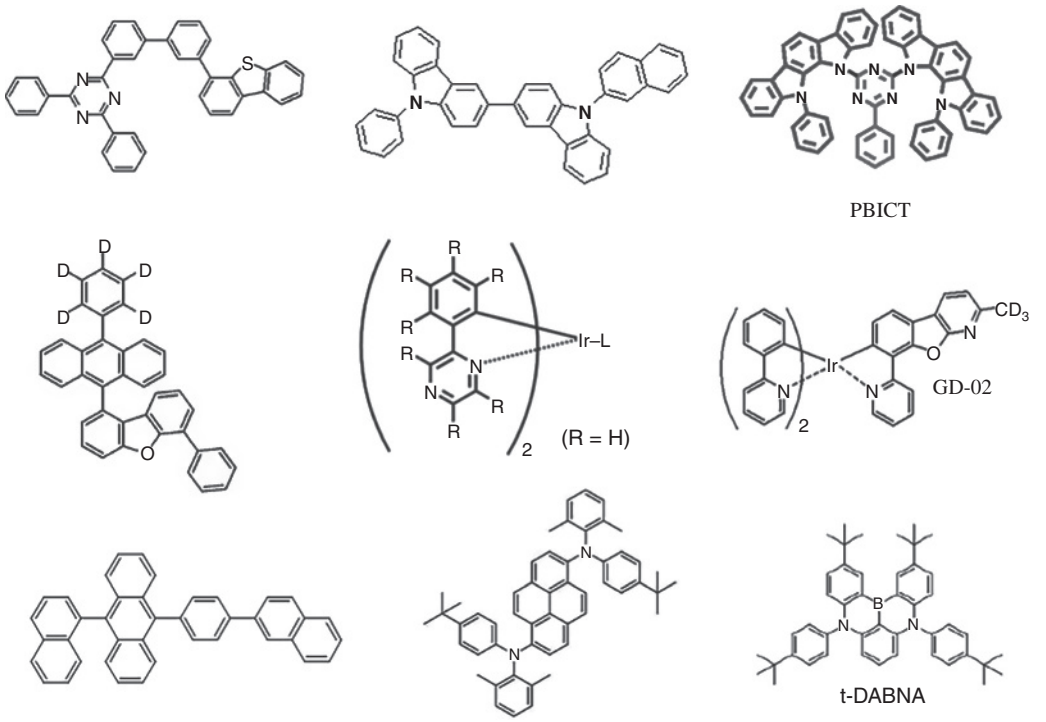

Figure 1.10 Examples of hosts and blue fluorescent, green, and red phosphorescent dopants.

3,5-triazine (PBICT) shown in Figure 1.10 [110]. This type of bipolar molecule as a TADF host was shown to be less sensitive to doping concentration, and when doped with the green phosphorescent dopant tris(2-phenylpyridine)iridium $[Ir(ppy)]_3$, PBICT is reported [111] to produce a maximum EQE of 23.9% at low doping concentration (~3wt%).

For doped blue fluorescence OLED (particularly the deep blue), the proper selection of a wide bandgap host material with sufficiently high solid-state PL is the prime concern. By many accounts, the best blue host molecules of today are still based on the core structure of di(aryl)anthracene (DAA) [112], which not only has an extremely high PL efficiency but also has the propensity of inducing significant TTA [113] to generate more singlet exciton (exceeding the theoretical limit of 25%). Nonetheless, there have been a few incremental improvements on DAA by substituting it with deuterated benzene as well as dibenzofuran [114] (for triplet exciton blocking). However, detailed structural information remains to be sketchy and guarded heavily as trade secrets by those Co's who invented them. One can only extract from what little (often fuzzy) information was disclosed in the open literature and patents from which a few archetypical examples are shown in Figure 1.10 for reference.

1.3.5.2 Deep Red Phosphorescent Dopants

Conventional Ir-containing phosphorescent dopants are mostly based on the ligands of 2-(phenyl) isoquinoline and 2-(phenyl)quinoline, like $Ir(piq)_3$ and PQIr, respectively. But their colors are neither deep enough to satisfy the new broadcasting television standard Rec. 2020 (or BT.2020) [43] with red chromaticity of $CIE_{x,y}$ (0.708, 0.292) nor the future demand of OLED lighting for the auto industry [115]. To shift to deeper red, a ligand with smaller bandgap energy ($\Delta E_{HOMO-LUMO}$) like

that of 2-(phenyl)pyrazine becomes necessary for the design of Ir-complexed dopants. As a result, most recent research has been focused on the improvement of color (deeper emission with narrow FWHM), efficiency, and high-temperature (85 °C) operational stability. One of the best EL performances reported to date is a doped emitter with a premixed-hosts system in a bottom-emission OLED that achieved 3.30 V and 3.08 mA cm^{-2}@ 500 nits with a luminance efficiency of 14.6 cd A^{-1}, EQE of 25.9%, and $CIE_{x,y}$ (0.708, 0.292) [116].

1.3.5.3 Deep Green Phosphorescent Dopants

For future displays, the new Rec. 2020 (also known as BT.2020) wide color gamut specifies 99.9% reproducibility of natural colors with a green chromaticity expanded to $CIE_{x,y}$ (0.170, 0.797). This deep green color standard proves to be a very tall order for most of the current green phosphorescent emitters to fill. For instance, homoleptic $Ir(ppy)_3$, which was the first iridium-based phosphorescent material reported for OLEDs, could only achieve a green $CIE_{x,y}$ of (0.27, 0.63) with an EQE of 8%, while the other well-known heteroleptic $(ppy)_2Ir(acac)$ produced a green $CIE_{x,y}$ of (0.31, 0.64) with an EQE of 12% in a bottom-emission device [117, 118]. While research is ongoing, the best solution reported to date appears to rely on several material and device improvements: (i) design and synthesis of new green phosphorescent dopant (like GD-1 shown in Figure 1.10); (ii) employing new electron-transport host molecule (ET-host) with sufficiently high triplet energy and electrochemical stability; (iii) adopting mixed electron-transport and hole-transport hosts of similar sublimation temperature and thermal property; and (iv) premixing these two hosts in proper ratio to induce exciplex formation and allow efficient ExTET to occur. Only when all these mutually dependent factors are working together in the device can a high-efficiency and long-lifetime deep green phosphorescent emitter be then produced. One of the best EL performances reported so far was a doped emitter with a premixed-hosts system in a bottom-emission OLED, which achieved EL performance of 3.30 V and 0.94 mA cm^{-2} @ 1000 nits with a luminance efficiency of 93.7 cd A^{-1}, EQE of 24.2%, and $CIE_{x,y}$ (0.338, 0.638) [119]. The best result of an accelerated driving-lifetime test with a constant current density of 50 mA cm^{-2} is reported to be T90 = 100 hours at an initial luminance of about 40 000 nits.

1.3.5.4 Deep Blue Fluorescent Dopants

Regardless of its relatively low exciton harvesting efficiency, fluorescent blue emitters are still widely used in present commercial OLED displays. This is mainly due to its long device lifetime, high material stability, and simple molecular design as compared to those of phosphorescence. The deep blue emitter has always been the holy grail of OLED as it impacts greatly not only on the color fidelity but also the overall power consumption and EL performance, including the backplane TFT design [120]. In the first decade of the twenty-first century, unusually high EL efficiencies have been reported for a few deep blue fluorescent materials, many of which are fluorophores based on an anthracene core [121]. A good example is the nondopant deep blue device using the **TAT** molecule with $\lambda_{max}^{EL} = 444$ nm, $CIE_{x,y}$ (0.16, 0.09), and EQE (η_{EXT}) = 7.18%, but its lifetime was short. Further study [122] has revealed that both TTA and the out-coupling enhancement by horizontal dipole orientation [123] of emitting molecules had contributed to the enhancement of η_{EQE} beyond what could be produced by normal fluorescence. By density function theory (DFT) and Spartan module simulation, a recent study [124] suggested that rigidity of fluorophore, small solvatochromic effect, suitable HOMO–LUMO level, and narrow FWHM are all important parameters to consider in the design of deep blue fluorescent dopants.

By all things considered, pyrene-based dopants [125] with 2,7-nitrogen-donating (amine) substituents appear to stand out as one of the best choices for the deep blue emitter (Figure 1.10). Strategic placement of aromatic amine auxochromophore group [126] is a good methodology to attenuate the HOMO level of the blue dopant, which renders more efficient Förster energy transfer to take place from a blue fluorescent host by dipole–dipole interaction. One of the best-reported EL performances of a stable pyrene-based deep blue dopant in a bottom-emission OLED is: 7.7 mA cm^{-2}@ 3.10 V, $CIE_{x,y}$ (0.140, 0.121), luminance efficiency = 10.4 cd A^{-1}, EQE = 10.7%, and LT90 = 180 hours @50 mA/cm^2. To satisfy the ultimate BT.2020 blue specification of $CIE_{x,y}$ (0.131, 0.046), a top-emission OLED with the desired micro-cavity structure is still needed, with which the blue chromaticity can be shifted deeper to $CIE_{x,y}$ (0.145, 0.046) [127].

Recent work [128] has shown that by incorporation of the isoelectronic [—B═N—] unit into a normal polyaromatic molecule with [—C═C—] as in 4b-aza-12b-boradibenzo[g,p]chrysene can effectively increase its bandgap energy ($\Delta E_{HOMO-LUMO}$) as well as the triplet energy (E_T). One of the best-reported cases is based on a vinylogous [—B═N—] derivative (tDABNA) shown in Figure 1.10, which achieved a deep blue chromaticity of $CIE_{x,y}$ (0.135, 0.072) [129] in a bottom-emission device. Another blue vinylogous-[BN]-based TADF emitter, DABNA-2 with a very small FWHM of 28 nm and PL λ_{max} = 467 nm, was reported to have achieved an EQE of 20.2% with $CIE_{x,y}$ (0.12, 0.13) [130, 131].

1.3.6 Encapsulation

Encapsulation is a must for OLED, which needs a hermitical seal to prevent moisture and oxygen from penetrating into the device and causing corrosion of reactive electrodes and oxidation of organic molecules. As glass is the best barrier material, most of the rigid OLED products of today have been protected by a glass cover [132] that is laser-sealed around the edge with glass frits to prevent lateral permeation. The disadvantage of glass-type encapsulation is that it is not only breakable but also adds considerable thickness (x2) and weight to the display. The edge area for glue also considerably reduces the display size, which is an important consideration for modern design of smartphones.

As AMOLED technology advances from rigid structures to ones of flexible form factors, from bendable and foldable to rollable, the transition from glass to TFE becomes ever more essential for FOLED applications. There have been several TFE structures reported in the literature where encapsulation layers are deposited as a combination of alternating inorganics (e.g. AlOx, SiO_2, SiNx, SiON) and organic polymers, among which the best known are Phillips NONON [133] and Vitex Barix® film [134]. In all of these technologies, the inorganic layers work as water diffusion barriers while the organics function as planarization and smoothing layers, which also aid to release the stress in the multilayer TFE stack. Increasing the thickness of silicon nitride and oxide layers greatly reduces pinholes and enhances the gas and moisture barrier property in the vertical direction. One of the most widely adopted methods to deposit the inorganics in the industry is the PECVD [135], though atomic layer deposition (ALD) as well as PEALD [136] has also received considerable attention due to its super step coverage. During the PECVD process, there are considerable particles being generated in the inorganic thin film (<1 μm) that needs to be covered by the organic layer (4—10 μm thick). The best way to deposit the organics appears to be ink-jet printing (IJP) [137] using the 100% solid UV curable type of ink, which has the capability of covering various edge shapes like notches and curved corners found in many of today's AMOLEDs.

The target WVTR for OLED is $1\times10^{-6}\,g\,m^{-2}day^{-1}$ (or less) at ambient temperature, which is well below the detection limit of many commercial instrumentations. To date, one of the most sensitive methods for measuring trace water permeation is the calcium (Ca) test [138], which is based on the observation of optical transmission of a thin film of Ca. When an opaque thin Ca film is reacting with water to form CaO or $Ca(OH)_2$, it will progressively become transparent, and from which, by correlation with the Beer–Lambert law, the rate of water permeation can be calculated. The most sensitive method reported to date for measuring moisture permeation is by radioactive tracer [139] using tritiated water (HTO) and subsequent scintillation counter, which can detect trace water levels as low as $3\times10^{-7}\,g\,m^{-2}day^{-1}$.

Finally, for future foldable OLED applications that require numerous bending usages over a very small radius in the hands of customers, none of the aforementioned TFEs may prove sufficient to provide failure-proof encapsulation. Several novel approaches that include the use of neutral-axis (NA) engineering, metal-based TFEs, and crack arresters [140] have been proposed to augment the existing TFE technology. Interested readers are referred to the references cited for further reading and in-depth study.

1.4 Device Structures

All good OLED materials described in the preceding sections invariably need good device structures to fully exploit, integrate, and maximize their best individual performances. This is particularly true in regard to overall EL performance involving key parameters of **s**tability, **p**ower (consumption), **e**fficiency, and **c**olor. Therefore, it can be said emphatically that *there is no good material without good device* and *there is also no good device without good material in OLED.* Throughout the history of OLED development, there have been many device structures that were ingenuously designed to maximize their EL performance, which are earmarked for specific applications such as mobile devices, TVs, and lighting. In addition to the basic *p–n* heterojunction bilayer and trilayer device architectures described earlier, there are a number of other important OLED structures of interest that are worth elaborating on here.

1.4.1 Multilayered Structure

As elucidated before, most of the voltage drop in driving OLED is caused by the large energy barrier that exists between the HOMO of the HTL and the work function of ITO (Φ_h) as well as the LUMO of the ETL and the work function of the metallic cathode (Φ_e) (see Figure 1.1a). This energy barrier can be largely moderated by inserting a HIL with a proper HOMO energy level lying between those of the anode and HTL as well as inserting an EIL with a proper LUMO between those of the ETL and the cathode [141]. Thus, the most robust small-molecule OLEDs of today, with the best EL performance, are found to contain a multilayered organic stack (as depicted in Figure 1.1b), in which the emitter layer contains one or two dopants (R, G, B) in a mixture of two host molecules (co-host) that preferably have bipolar transport properties [106–109]. It is perhaps for this reason (among others) that small-molecule OLEDs fabricated by thermal evaporation have enjoyed greater success than those of the polymer (PLED) or other solution-processed devices to date. This is because that by thermal evaporation one can readily fabricate as many layers (as thin as 1 nm) as necessary, while it would be mission impossible by solution processing. This is

particularly true for phosphorescence devices where additional hole-blocking, electron-blocking, and exciton-blocking layers may be necessary in order to enhance device stability and alleviate efficiency roll-off [142].

1.4.2 Graded Junction Device

There were reports suggesting that the heterojunction created by two adjacent organic layers with vastly different HOMO/LUMO energy levels may result in considerable charge built-up upon extended driving, which can be detrimental to long-term device operational stability [143]. A graded mixed emission layer containing both HTMs and ETMs was reported to reduce the electric field caused by accumulation of charge at the interface and decrease the probability of *Joule* heating, thereby increase the lifetime of the device [144]. To eliminate the creation of a heterojunction interface, and at the same time, enhance the balance of charges, a concept of a fuzzy-junction (cross-faded emission layer) structure with composition that varies continuously has been proposed [145, 146]. This type of device structure somehow did not get the attention it deserves for further development and manufacturing, which may be due in part to its more complicated tooling and difficulty in controlling thermal evaporation by precise movement of the substrate in relation to three evaporating sources in a vacuum [147].

1.4.3 *p–i–n* Structure

To reduce the power consumption of OLED, it is important to keep the organic stack thin. But, often in production, too thin a multilayer device would often impact on device stability and the production yield, as it is more difficult to control the uniformity over a large area in process engineering. Besides, ITO/glass with sufficient conductivity does not always have a smooth surface on which to deposit organic materials. Therefore, a much thicker HIL is often needed in production, which is particularly acute in PMOLED manufacturing. Additionally, in lighting applications, power consumption is also the utmost consideration for WOLEDs in order to compete with LED type of SSL. Thus, there's a continuing need in industry to keep the drive voltage low by both improving the efficiency of OLED materials and device structure.

Today, the best solution to lowering drive voltage is the *p–i–n* structure in which relatively thick HIL and EIL are doped by strong electron acceptors (*p*-type) and donors (*n*-type), respectively. Due to the electric doping in HTL and ETL, the increased conductivity of the organic stack induces band bending at the interface. As a result, it also reduces carrier–injection energy barriers as well as operating voltage. Figure 1.11 illustrates the band bending diagram caused by electron transfer from the HOMO of HTM to the LUMO of the *p*-dopant at the anode, and likewise the electron is withdrawn from the HOMO of the *n*-dopant to the LUMO of ETL [148, 149]. The net effect is that the conductivities of both the HTL and ETL are increased dramatically, and so is the ease of hole and electron injection (by tunneling) [150] from the anode and cathode, respectively.

As described before, the most widely used *p*-dopants are F_4-TCNQ, HAT, and [3]-radialene, with their LUMO levels (electron affinity) more negative than −5.2 eV, which is close to the ionization energy of most HTMs (see Figure 1.8). But the *n*-type dopants (with HOMO above −4.0 eV) are usually unstable in air and difficult to handle. It appears that one of the most widely employed *n*-dopants is still Li metal and its derivatives, like LiF and Liq, that can presumably be reduced in situ to generate Li^0 in contact with the cathode (e.g. Al) [151] during evaporation in a vacuum.

The question of stability and operational lifetime is an important issue for *p–i–n* OLED, as dopants may diffuse to the EML to produce potential luminance quencher, particularly for Li-doped

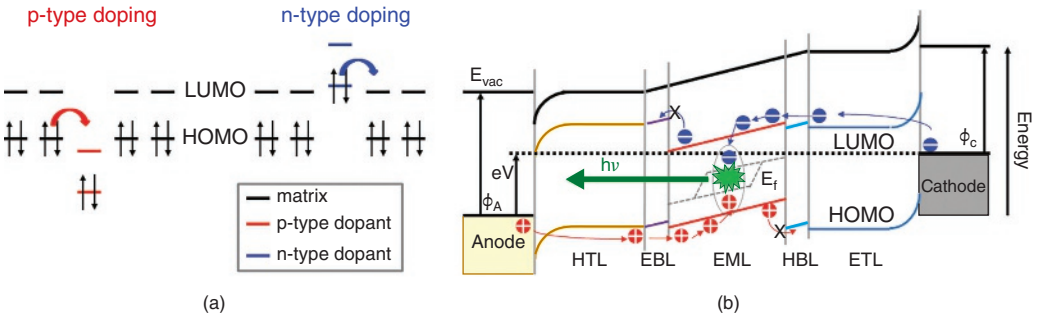

Figure 1.11 Schematic energy diagram of **(a)** Charge carrier transfer from *p*- and *n*-type dopants to their host matrix materials. *Source:* Reproduced from [148, 149] / with permission of American Chemical Society. **(b)** Functionality of a *p–i–n* OLED structure under operation. *Source:* Reproduced from [152] / with permission of American Chemical Society.

device. The insertion of a thin hole-and electron-blocking interlayers is crucial to confine the injected charges and ensure good charge balance within the EML (Figure 1.11b) [152]. The advantage of extremely low operating voltage and high luminous efficiency of *p–i–n* structure also paves the way for the development of both high-resolution AMOLED displays and power-efficient lighting. As the increase of voltage drop over the entire doped transport layer is minimized, it opens the way to optimize the thickness of the charge transport layer without impacting on resonant light out-coupling for top-emission OLEDs with strong micro-cavity effects, which will be described later.

1.4.4 Bottom- and Top-Emission Structures and Transparent OLED

Bottom-emission OLED (Figure 1.12a) is the most common device structure where light emits from the bottom substrate, which consists of a reflective cathode, a transparent anode, and various functional organic layers sandwiched in-between. When the device is turned on, the light generated in the organic EML will penetrate through the transparent bottom anode (e.g. ITO) substrate and be reflected from the thick metallic cathode, then escape out of the bottom into the air. Generally, the light out-coupling efficiency of a planar Lambertian emissive source follows the Fresnel equation depending on the refractive indices of the media as described before.

However, in the case of high-resolution AMOLEDs, the internal luminance operating point is governed by the aperture ratio at each pixel, which impacts greatly on the EL performance, particularly on the lifetime. For instance, the opaque LTPS pixel circuits with luminance compensation could contain as many as seven transistors and two capacitors (7T-2C), thus occupying considerable space (>60%) on the TFT backplane, which results in a low aperture ratio of less than 40%. Therefore, a top-emission OLED (TOLED) structure that allows light to emit from the top surface of the device is very important in AMOLED. As depicted in Figure 1.12b, when the anode is made reflective and the cathode is a semitransparent metal, the generated light will emit from the top cathode side, thus avoiding the shielding effect of the opaque TFTs at the bottom altogether.

The disadvantage, however, is that TOLED is more complicated and difficult to fabricate than that of the bottom emission, particularly in mass production involving a very large substrate. This is because the semitransparent cathode is a very fragile, thin metal, usually around 15 nm or less, which needs to be treated with great care. To enhance the transparency of the semitransparent

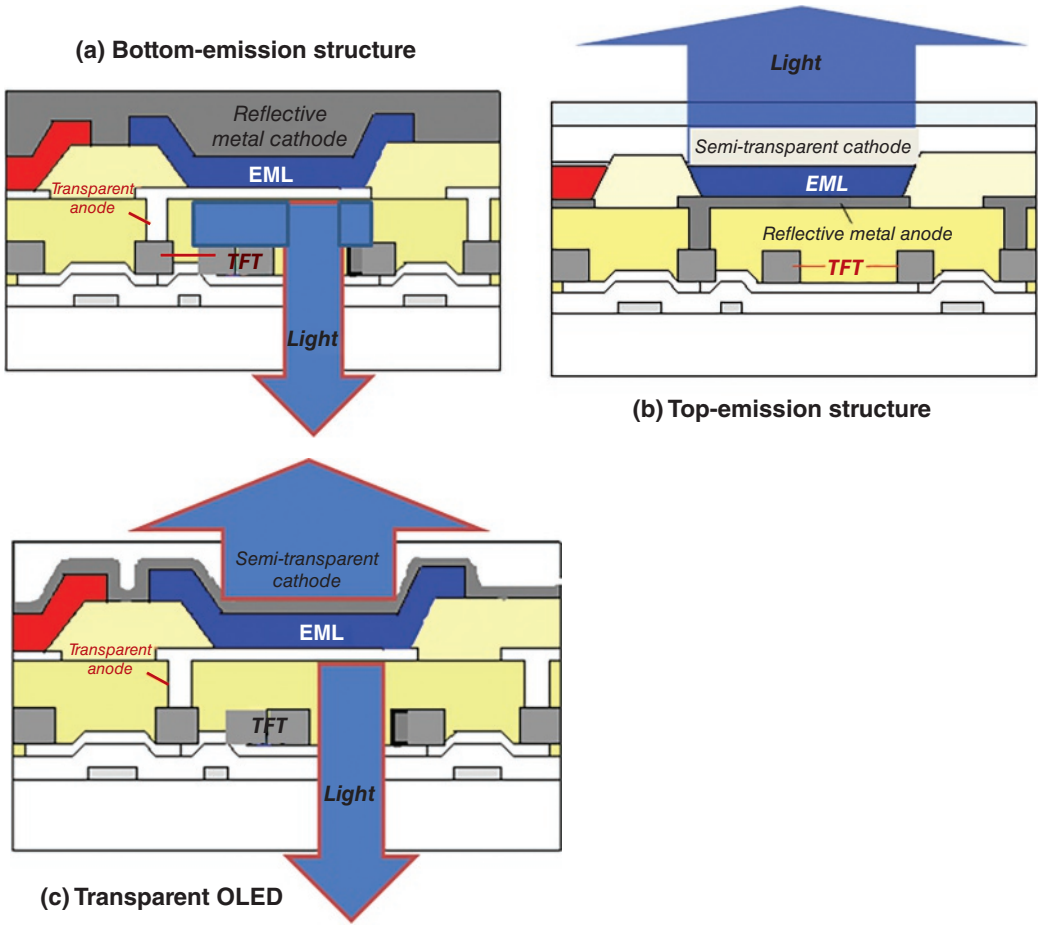

Figure 1.12 Schematic diagrams of **(a)** bottom-emission, **(b)** top-emission, and **(c)** transparent AMOLED structures.

metal (e.g. Ag, Mg), a capping layer (CPL) [151] with matching refractive index, like TiO_2 ($n \sim 2.3$), SnO_2 (2.1), and TeO_2 (2.2), is often overcoated to protect the thin cathode before being subjected to further processing and encapsulation.

If the anode is also transparent, or better yet, the TFT backplane is transparent like that of indium–gallium–zinc–oxide (IGZO), light can emit from both sides of the device. Then, this kind of OLED is called a transparent OLED, as shown in Figure 1.12c. The advantage of this structure is that the device is near-transparent in an ambient light environment when off. But once it is lit, information can be displayed, making it very flexible and convenient in design and application. This property, with its great freedom of design and free form factor, is also quite unique to OLED that is not readily attainable by other display technologies. The world's first large-size 77-in transparent flexible OLED TV with ultrahigh definition (UHD), which can be rolled up to a radius of 77 mm with a transparency of 40%, was recently showcased by LG on the a-IGZO TFT backplane and transparent PI [139].

Besides its high aperture ratio, one of the best advantages of TOLED over that of the conventional bottom-emission OLED is that the creation of micro-cavity within the reflective anode and

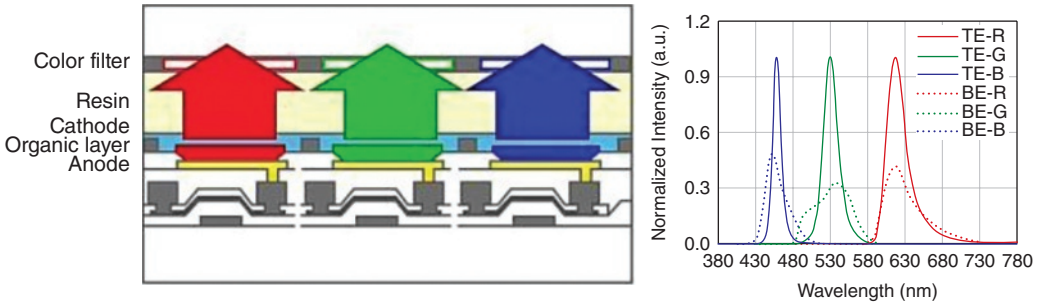

Figure 1.13 Spectral narrowing and intensity enhancement effects in TOLED with RGB optical path length adjusted micro-cavity. *Source:* Reproduced from [157] / with permission of John Wiley & Sons.

the semitransparent cathode. This optical effect can be greatly exploited to compensate the shortcomings of RGB emissive materials in AMOLEDs to produce very saturated colors that could not be obtained otherwise. The micro-cavity effect of OLED can be simulated as one particular kind of Fabry–Perot filters that satisfies Eq. (1.1),

$$\frac{2L}{\lambda_{\max}} + \frac{\Phi}{2\pi} = m(m = \text{integer}) \tag{1.1}$$

where L is the optical length between the two mirrors and Φ is the sum of the phase shift from anode and cathode [153]. The FWHM [154] can be estimated by Eq. (1.2).

$$\text{FWHM} = \frac{\lambda^2}{2L} \times \frac{1 - \sqrt{R_1 R_2}}{\pi (R_1 R_2)^{1/4}} \tag{1.2}$$

where R_1 and R_2 are the reflectance of the two mirrors. Spectral narrowing and intensity enhancement are two of the most common phenomena caused by the micro-cavity effect in TOLED as graphically illustrated in Figure 1.13. By proper adjustment of the optical length of the respective R, G, and B emitters in the TOLED structure [155], color purity [156] and efficiency can be improved greatly.

1.4.5 Tandem OLED Structure

A tandem OLED structure is formed by connecting several independent OLEDs in series, with the purpose of enhancing the current as well as the quantum efficiency of the device, albeit at the expense of drive voltage. Nevertheless, multiple photons per unit charge can be generated by the tandem structure depending on the number of stacks. It is also conceivable that WOLED of high luminance can be generated by stacking individual OLEDs with different colors like R, G, and B. The main advantages of the tandem concept are the enhancement of lifetime and brightness for the reduction of the applied current [158]. This is because the current density (J) for each of the single unit cell is not changed while the brightness (L) of the combined units will be multiplied by the number of cells interconnected. However, the power efficiency of such a device can never be higher than that of a conventional device, because the operating voltage is also increased proportional to the number of stacked units as illustrated in Figure 1.14.

It is clear that selecting a pair of suitable "*n/p*" type of materials for the CGL connecting the individual units of the device are crucial for realizing tandem OLEDs. Some of the notable CGLs

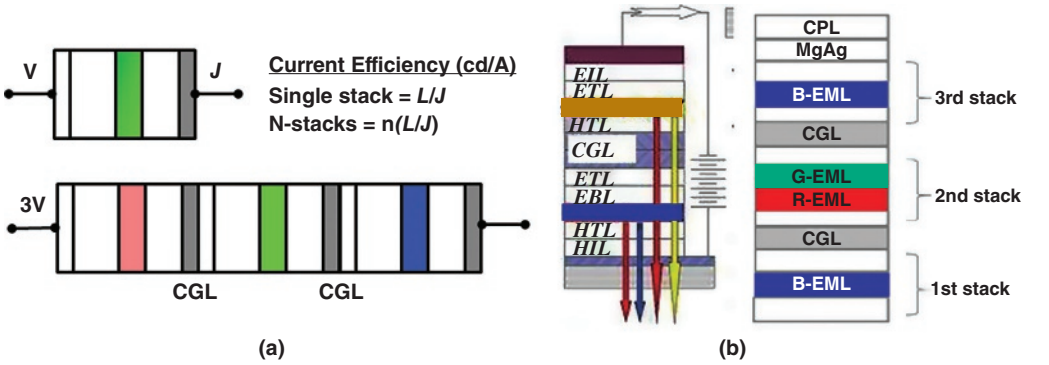

Figure 1.14 Illustration of **(a)** single versus tandem OLEDs and **(b)** hybrid tandem WOLED with one and two CGLs structures. *Source:* Reproduced from [163] / with permission of John Wiley & Sons.

that have been reported were Cs:BCP/V_2O_5 [159], Alq_3:Li/NPB:$FeCl_3$ [160], Mg:Alq_3/WO_3 [161], and Li:BPhen/HATCN [162]. The principle of CGL based on double layers of highly *p*- and *n*-doped organic transport layers can be interpreted using qualitative energy levels of doped transport layers. With effective doping, the Fermi levels within the *p*- and *n*-doped transport layers are close to their HOMO and LUMO, respectively. If they contact with each other, a common Fermi level throughout both layers is established by equilibrium. When an external bias is applied to a tandem OLED, the *p*–*n* junction is actually operating under a reverse bias, which lowers the LUMO states of the HTL to the unoccupied LUMO states of the ETL. Then these electrons will immediately be driven away from the interface by the external electric field and be injected into the other emission layer. The holes left in the HOMO states of the HTL are in the same way injected into the emission layer of its own emission unit.

For lighting application [163], a hybrid tandem WOLED (see Figure 1.14a), which combines blue fluorescence EL unit and green and red phosphorescent EL unit by CGL, is a good way to achieve improved quantum efficiency and lifetime. The blue fluorescence EL unit is a critical component in determining the color gamut, efficiency, and lifetime of the hybrid tandem WOLEDs, as nearly all of the blue phosphorescence materials (and their devices) reported to date were not robust enough for the stringent requirement of lighting.

Recently, TOLEDs with a wide-color gamut and high efficiency have successfully been fabricated by using a three-stacked B/RG/B tandem structure with two CGLs and a color filter [157]. With a semitransparent Mg:Ag cathode and indium zinc oxide (IZO) as a CPL, they achieved 90% color gamut coverage of the UHDTV standard BT.2020 while maintaining high current efficiency of R ~15.5 cd A^{-1}, G ~ 26.6 cd A^{-1}, and B ~ 3.5 cd A^{-1} (Figure 1.14b).

1.4.6 PM Addressing

One of the first OLED display products that entered the marketplace was in 1997 by Pioneer, who introduced a small car stereo multi-area color display in Japan based on the PM array of low resolution. In PMOLEDs, individual pixels are defined by the overlap of ITO columns (anodes) and metal rows (cathodes) as illustrated in Figure 1.15a, in which anodes are patterned by the usual wet lithography. But patterning air-sensitive cathodes requires a new technique [164] that involves the direct evaporation of metal under vacuum onto rows of "cathode separators" that are prefabricated on ITO/glass prior to thermal deposition. Relatively, they are easy to fabricate and well-suited

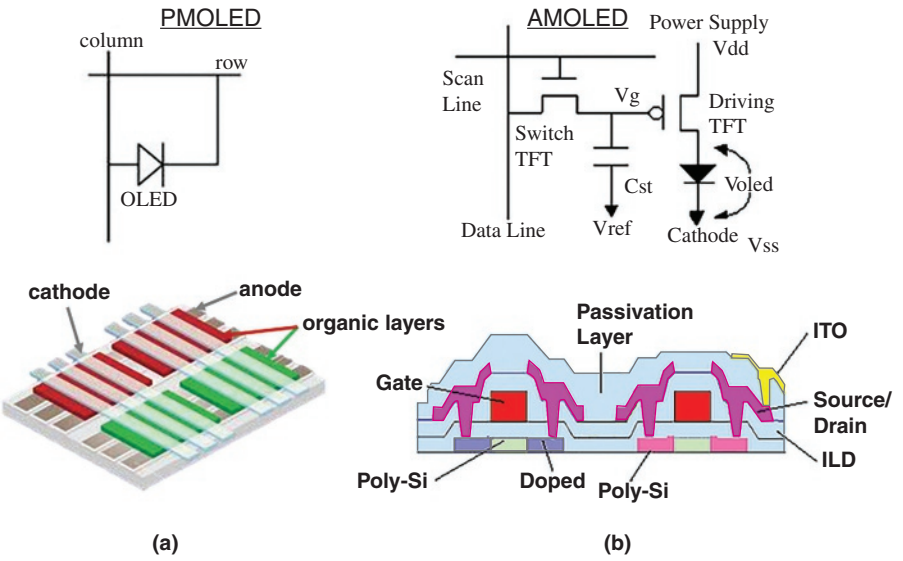

Figure 1.15 **(a)** PM and **(b)** LTPS TFT AM OLED. *Source:* Reproduced from [166] / with permission of John Wiley & Sons.

for small size, low cost, and low information-content applications such as alphanumeric, area color sub-displays used in many OLED watches. The downside of PM addressing is that they require pixels row-by-row scanned and driven under pulsed conditions to extremely high brightness, which invariably imparts great stress on OLED materials, thus shortens device lifetime. In addition, power consumption of PMOLED displays increases sharply with size, and both resistive losses in the conductive tracks and efficiency reduction for the diodes at high current densities limit the maximum number of pixels fabricated in the panel [165]. As a consequence, the size of full-color PMOLED displays is usually limited to smaller than 2 in.

1.4.7 AM Addressing

Differing from PMOLED, AMOLED displays use an integrated electronic backplane as their substrate, which comprises at least two TFTs and one capacitor (2T-1C) connected to each pixel, with one of the TFTs functions as a switch and the other controls the current fed through the diode. These elements are incorporated primarily to create a sharp threshold to improve the multiplexibility of the display. They are capable of transferring maximum charge to the pixel capacitance during address time and disenable any significant leakage during frame time. AM addressing scheme has many advantages over that of PM, such as no crosstalk, continuous excitation, low-power consumption, continuous cathode configuration, and integrated drive electronics. Thus, coupling with its lightweight and thin and flexible form factor, AMOLED functions exceptionally well in various sizes of high-resolution, high-information-content applications such as high-speed video games, HD movies, and graphics that are particularly suitable for use in 4G–5G smartphones.

Unlike the driver of a liquid crystal pixel that can be voltage-switched using a single “address” transistor, the current-controlled emission of an OLED pixel requires at least two transistors to maintain the necessary continuous diode current in the emitting state. As an example of a

polycrystalline silicon (poly-Si) AM pixel circuit and TFT architecture illustrated in Figure 1.15b, the driving transistor provides the current for the OLED, and is operated in saturation to overcome its threshold voltage variation. The switching transistor acts as an on/off switch to sample and hold a voltage on the gate of the driving transistor.

1.4.8 TFT Backplane Technologies

For AMOLED to realize all its attributes and deliver superb performance, it needs to integrate both an OLED frontplane (as described in the previous sections) and a TFT backplane. Table 1.3 compares three of the major TFT technologies that have been exploited in AMOLED [167].

***a*-Si TFT**. Without a doubt, amorphous silicon (*a*-Si) TFT is the most mature and abundant, which has been widely used in the fabrication of LCDs due to its ease of scaling (up to Gen 10.5 fab is available in China and Korea), low cost, high yield, and good uniformity. But, its mobility is low ($<1\,cm^2V^{-1}s^{-1}$), nor is its large threshold voltage shift ($\Delta V_{th} > 5\,V$) upon stress and ageing suitable for an OLED backplane, even though there has been much effort in trying to overcome its deficiency by clever drive circuit compensation [166, 168].

LTPS-TFT. LTPS, which can be manufactured on a glass substrate at relatively low temperature, is best suited for small-to-medium-size AMOLEDs that are fabricated by the SBS FMM RGB patterning process. Depending on grain size and the process by which poly-Si grain is crystallized from *a*-Si, its mobility can be as high as $\sim 100\,cm^2V^{-1}s^{-1}$, which is more than enough to drive OLED, particularly with the high-efficiency phosphorescence materials and *p–i–n* device structure. In addition, LTPS-TFT is stable with very low ΔV_{th} shift ($<0.5\,V$) during operation, which is particularly important for OLED that is extremely sensitive to the slightest amount of drive current variation caused by the swing of threshold voltage.

Several techniques are available for the crystallization of *a*-Si films, which include low-temperature solid phase crystallization (SPC), excimer laser annealing (ELA), and metal (usually Ni)-induced crystallization (MIC). SPC offers improved performance at the expense of low throughput, while MIC could result in high leakage currents due to the presence of traces of residual metals left in TFTs. ELA can form poly-Si grains of excellent structural quality, but it demands very tight control to avoid spatial nonuniformity, which often suffers from a rather narrow process window in manufacturing. However, its grain-size variation can be reduced by using multiple laser shots [169], which produce a TFT backplane with sufficient yield and a large enough grain size that have proven production worthy in AMOLED manufacturing. But LTPS is costly, and it has been difficult to scale up to over Gen 6 ($1500\times1850\,mm^2$). Besides, the uniformity of LTPS formed by ELA in

Table 1.3 Comparison of major TFT technologies.

Items	*a*-Si TFT	Poly-Si TFT	Oxide TFT
Semiconductor	Amorphous Si	Polycrystalline Si	Amorphous IGZO
Channel mobility	$1\,cm^2\,V^{-1}\,s^{-1}$	$\sim 100\,cm^2\,V^{-1}\,s^{-1}$	$10 \sim 40\,cm^2\,V^{-1}\,s^{-1}$
TFT for OLED	4 ~ 5	5 ~ 11	4 ~ 5
Pixel circuit	Complex (>4 T)	Complex (>4 T)	Simple (2T + 1C)
Stability (ΔV_{th},100 khr)	>5V	<0.5V	NA
Pixel TFT	NMOS	PMOS (CMOS)	NMOS

production is still difficult to control, particularly for large-size substrates. The overlapped laser beam line-scanning during the ELA process can cause incidental protrusion on the surface of poly-Si film, which leads to nonuniform electrical characteristics and the streaking mura that is the primary cause in limiting AMOLED manufacturing yield in the early days [170]. Mura can be suppressed by the refined and modified ELA process [171] based on the two-shot sequential lateral solidification process to smooth out the surface roughness of poly-Si film.

But, for high-resolution and image-quality AMOLED, the slight yet detectable pixel-to-pixel luminance nonuniformity remains to be a critical issue that needs to be resolved. This is mainly due to the swing in TFT threshold voltage and mobility, which lead to variation of drive current that eventually determines the pixel luminance of OLED. Elaborate internal [172] and external pixel compensation circuits [173] must therefore be added in the drive electronics along with many additional TFTs as well as capacitors designed in the backplane for each pixel in order to produce a perfect display image.

Oxide TFT. In order to be competitive with LCD in the TV market, OLED needs a compatible TFT backplane technology that is cost-effective, robust, and most of all scalable to Gen 10.5 ($2940\times3370\,mm^2$). Although the current ELA LTPS-TFT backplane has widely been used commercially to manufacture small-to-medium-size AMOLEDs, scaling to larger-size substrates (> Gen. 6.5) has proven to be very difficult and nonprofitable due primarily to cost and yield issues. Alternatively, amorphous oxide TFTs with their exceptional good attributes [174] (shown in Table 1.3), such as relatively high field-effect mobility (typically $10–20\,cm^2V^{-1}s^{-1}$), low off-state current (~pA), high uniformity over a large area (up to Gen.10.5 substrate), and high transmittance (~90%) for visible light, are particularly suitable for large-size OLED TV production [175]. In addition, the low processing temperature (<350 °C) is also most conducive for flexible OLED manufacturing based on PI substrate. Among the many metal oxide semiconductors that have been studied, amorphous indium–gallium–zinc–oxide (*a*-IGZO) TFT stands out as the most robust and manufacturing worthy, even though its average *n*-channel field-effect mobility has rarely exceeded $20\,cm^2V^{-1}s^{-1}$. As the resolution of future TV increases to 8K and frame rate boosts up to 240 Hz, the field-effect mobility of oxide TFT needs to be improved further. There are a number of methodologies that have been studied to increase the *n*-type field-effect mobility of oxide TFT, namely oxygen vacancy modulation, doping (e.g. Nd, Y, Sr, Zr, Hf), plasma treatment, laser, and microwave annealing [176]. Recently, a lanthanide rare earth-doped IZOTFT [177] with the BCE process is reported to exhibit high field-effect mobility of about $40\,cm^2V^{-1}s^{-1}$ and a subthreshold swing of 0.13 V/decade with an $I_{on}/I_{off} \sim 10^9$. One of the highest mobilities reported so far appears to be the tin-doped zinc oxide (TZO) TFT, which is vacuum prepared by RF magnetron sputtering with a specific oxygen partial pressure of about 10% to achieve a mobility of $66.7\,cm^2V^{-1}s^{-1}$ with a low off-current of 3 pA, a high current on/off ratio of 2×10^7, and a low subthreshold swing (S.S) of 333 mV dec^{-1} [178].

Contrarily, *p*-type oxide TFTs are still in an early stage of development and their mobility is only around $2\,cm^2V^{-1}s^{-1}$. As a result, it would be quite a while before complementary metal oxide semiconductor (CMOS) logic circuitry based on *n*- and *p*-type oxide TFTs can be realized in OLED displays.

LTPO TFT. Low-temperature polycrystalline silicon oxide (LTPO) TFT technology [179] was recently developed as a backplane for wearable AMOLED displays in the Apple Watch Series 4. It takes advantage of both the high mobility and low threshold voltage shift (ΔV_{th}) properties of LTPS and that of the ultra-low off-stage leakage current (I_{off}) of IGZO to enable significant display frame rate and power reductions without jeopardizing image quality. To maximize LTPO TFT performance, Apple has developed a new 6T-1C pixel circuit design that is composed of one oxide TFT

and five LTPS TFTs. In this circuit, the oxide TFT is used as the switching transistor to control programming, while one of the LTPS TFTs serves as the driving transistor to generate the precise current to drive the OLED, and the rest of which serves to control power, initiation, and data signals. Reducing the leakage currents that discharge from the storage capacitor (C_{ST}) through the switching metal oxide transistor proves very effective in achieving a low refresh rate. The proposed pixel design takes advantage of the ultra-low I_{off} of metal oxide TFT by replacing a conventional LTPS switching transistor with an oxide transistor, which ensures minimal discharge of C_{ST} while the pixel is in the emissive phase and the switching transistor is off.

To reduce the number of masks and processing steps, Apple opted to use a bottom-gate LTPO TFT structure that shared the same layer of gate electrodes with those of LTPS. But, due to the shared gate structure, interactions between LTPS and oxide TFT processes are unavoidable, which require careful manipulation to avoid unwanted behavior in both types of TFTs. Extreme care during processing must therefore be taken to passivate the poly-Si grain as well as the poly-Si/gate insulator and to control interfacial defects of LTPS TFT by hydrogenation without damaging metal oxide TFT. For it is well known that excess hydrogen ions can diffuse into metal oxide channel to combine with oxygen dangling bonds or break oxygen–metal covalent bonds to form hydroxide, which will ultimately change the distribution of the oxide density of states, resulting in a greater ΔV_{th} shift [180]. It was reported further that by utilizing LTPO TFT technology, the AMOLED can be operated at a frame refresh rate as low as 1 Hz without any perceivable luminance change and artifacts due to driving TFT hysteresis.

1.4.9 Inverted Device Structure

Considerable efforts have recently been directed toward the development of inverted type of OLEDs (IOLEDs), in which the roles of anode and cathode are reversed. For instance, the high work function transparent ITO in the bottom-emission OLED will now assume the role of cathode to inject electron while the low work function reflective metal (e.g. Al) injects hole. There are a couple of distinct advantages for IOLED: (i) since the usual extremely sensitive EIL that contains low work function alkali metal (e.g. Li, Mg, Cs) is placed at the bottom prior to the fabrication of organics, it provides a possibility of realizing an air-stable OLED [181] that no longer needs stringent encapsulation [182]; (ii) for future application of flexible large panel OLEDs, inverted structure allows the adoption of *n*-type transparent oxide (e.g. IGZO) TFT backplane that can be mass produced by sputtering at low temperature (below the T_g of most plastic substrates). This is because IOLED provides a bottom cathode structure that can be connected to the drain of the *n*-channel-driven oxide TFT, through which the compensation circuit of the TFT can be decoupled from the resistive loss of the OLED materials due to aging, and thus will not be impacted by the usual voltage swing [183].

Conventional bottom-emitting OLED is fabricated by starting with a transparent ITO for the anode, and an opaque reflective metal for the cathode, such as LiF/Al, while for bottom-emission IOLEDs, ITO is inverted to function as the cathode. This creates considerable problems as electron is difficult to inject from ITO into the organic layer due to their severe energy levels mismatch, which would cause the drive voltage to rise sharply and efficiency to fall. To facilitate electron injection from ITO, several new elements of EIL have been reported, such as ZnO/poly(ethylene imine) [184], Al/LiF/LG-201 [185], and ITZO [186].

An example of this type of device [187] is illustrated in Figure 1.16a, in which a conventional C545T-doped Alq green fluorescence OLED is compared with that of IOLED with the *n*–*i*–*p* structure, and in (b), by using *n*-doped ETL (Cs_2CO_3/BPhen) and *p*-doped HTL (WO_3/NPB), both carrier injections are enhanced from ITO and Al, respectively.

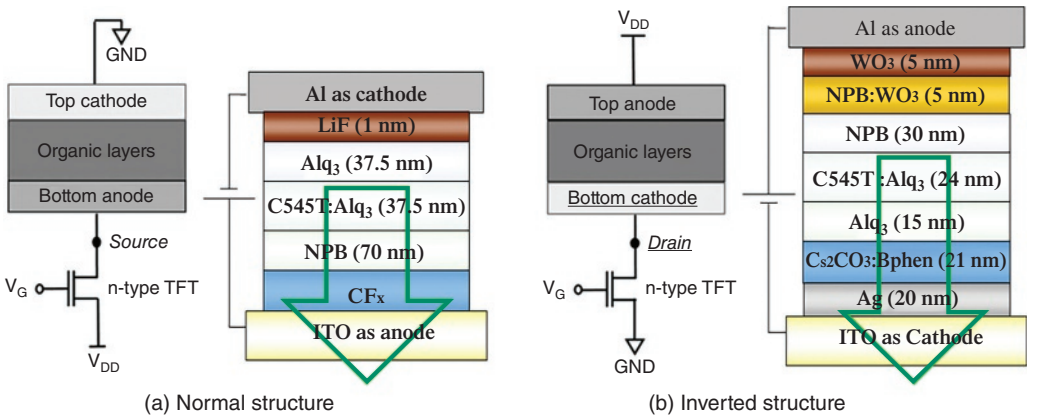

Figure 1.16 Sketch of an inverted bottom-emission OLED **(b)** is compared with a normal structure **(a)**. *Source:* **(a)** Reproduced from [183] / with permission of John Wiley & Sons, **(b)** [187] / with permission of Elsevier.

1.5 OLED Applications

Thanks to more than 40 years of relentless pursuit and ingenious R&D contributed by a great many scientists and engineers throughout the world, the performance of OLED has improved steadily, making it one of the premium choices of display for the consumer electronic (CE) products. According to a recent survey by Display Supply Chain Consultants (DSCC) [188], OLED is gaining significant ground in the display market, and their revenues are predicted to rise at a 10% CAGR from $28 billion in 2019 to over $50 billion in 2025. Not surprisingly, smartphones are its greatest success, which is followed by OLED TV, a long-distant second (<10% market share). This is because OLED is getting a boost from 5G due to its low-power consumption, thinner/free form factor, and lightweight, which offset the increased thickness, power, and weight of 5G components. So far, more than 80% of 5G smartphones have adopted OLED (driven mainly by the demand of flexible OLED), which is poised to overtake LCDs in the smartphone market as the dominant player in 2024.

Future expansion is expected to be found in automotive, tablets (driven mostly by folding OLED), notebooks, monitors, and AR/VR wearable displays. In addition, owing to the significant improvement in power efficiency (due to the advance in out-coupling technology) and panel reliability, OLED lighting is also to become an important growth driver both in automotive and indoor lighting applications [189].

1.5.1 Flexible OLEDs

Few would doubt that flexible displays may just be the "killer application" for which OLED has long been striving. Indeed, in nearly all market surveys, most of the popular CE display products – be that in smartphones, tablets, notebooks, monitors, smartwatches, or TV – now require some kind of "flexibility" in forms and shapes for which OLEDs are deemed by many experts to be the best (Figure 1.17). This is because, compared to LCDs, flexible OLEDs are much thinner, lighter, more power efficient, better in viewing angle and color accuracy, with unsurpassed contrast and true black, and above all, nearly unbreakable. They can be bended, curved, rounded, folded, and rolled to provide a great number of innovative designs and new

Figure 1.17 Examples of recent OLED displays and lighting products. *Source:* Reproduced from [194] / with permission of John Wiley & Sons.

screen geometries. They also have a very fast response time, which enables the new higher 90 Hz and 120 Hz screen refresh rates in smartphones, thus greatly improving image scrolling and videos, plus motion, and gaming performance.

1.5.2 Smartphones

The key element for a great smartphone has always been its truly innovative and top-performing display, and the best leading-edge smartphone of today is no doubt the Galaxy S20 Ultra marketed by Samsung in 2020. The flagship S20 has the latest dual-edge curved 6.9 in screen of flexible top-emission AMOLED, which is fabricated on a PI substrate using an LTPS TFT backplane and the precision FMM SBS RGB pixelation technology. It sports a new display form factor with a new aspect ratio of 20:9, which is 25% larger than that of 16:9 on most other smartphones because the display now has the same overall shape as the entire phone. It also sports a 3K (3200 × 1440) high resolution with 510 ppi, and a diamond pixel configuration with sub-pixel rendering for enhanced sharpness and higher peak brightness. According to a recent report by Display Mate laboratory [190], this new OLED has achieved a record-setting absolute color accuracy that is visually indistinguishable from perfect. It further concludes that "OLED displays now have tremendous performance advantages over LCDs, so high-end smartphones need them in order to compete at state-of-the-art performance levels, securing OLED as the definitive premier display technology for top-tier smartphones in the foreseeable future. With the continuing improvements in OLED hardware performance, picture quality, and precision accuracy, it will be much harder for new display technologies to challenge OLED."

1.5.3 Wearable OLEDs (Smartwatches)

Flexible OLEDs are an ideal technology for smartwatches because they are thin/light displays that can be manufactured and cut into various shapes and sizes of small watch screens (typically ~1.5 in across) with high resolution (>320 ppi) and 24-bit color. They offer much better black levels,

viewing angles, and, particularly, power management compared with those of LCDs. The power efficiency is the most important consideration of a smartwatch display because it is the single biggest power drain for the watch and thus determines the size of battery that is needed to keep it running for at least a full day. That is why Apple adopted the power-saving LTPO backplane technology in its Apple Watch Series 4, as described before, which won the Displays of the Year Award of SID [191].

1.5.4 Foldable OLED

Although initial volumes for the foldable OLED market are small due to some sporadic reliability issues around the hinges that remain to be resolved, few could deny that it is the next big thing for mobile device in the future. Samsung, in particular, considers its foldable OLED display as a stepping stone in revolutionizing display form factors with the global launch of the Galaxy Fold in 2019 [192]. This first-of-its-kind device (shown in Figure 1.17) bridges a smartphone and tablet with the help of two AMOLED displays, i.e. a 4.6-in external screen and an internal screen that expands to 7.3 in when unfolded. That interior display's size gives way to a powerful multitasking feature by operating three applications simultaneously. It also has a picture quality of up to Quad Extended Graphics Array ($QXGA^+$) resolution and a pure color gamut and peak luminance of up to 600 cd m^{-2}, letting users fully immerse themselves in various types of content such as gaming and video streaming. To achieve these specifications, Samsung adopted many highly efficient and reliable organic electroluminescent materials as well as highly durable mechanical components.

To make an inward foldable display with a bending radius of 1.5 mm, all the layers within the panel should be folded without causing any cracks. As a result, the foldable display employs a cover window made of flexible, hardened plastic, which reduces the display thickness by more than 50%. Furthermore, the stress of various layers (including the TFT, organic layers, polarizing plate, and cover window) must be appropriately relieved, allowing the product to pass a strict bending test of more than 200 000 cycles. A number of panel makers (e.g. LG, BOE) have opted instead for the outward-bending foldable OLED for use in the next-generation smartphones like the Huawei Mate X. But detailed technical information is still sketchy and unavailable.

Not to be outdone, Lenovo also has introduced its ThinkPad X1 foldable PC, which combines a notebook computer with a tablet [193]. When unfolded, the X1 Fold has a 13.3-in, 4:3 OLED display with a flat and firm surface and a touch screen made by LG. It is reported that Lenovo has spent four years developing the hinge, which gives the display a gentle radius when closed. Functionally, one can arrange to do your typing on a soft keyboard or use a Bluetooth keyboard that magnetically mounts inside the folded X1 Fold and charges itself from the PC.

1.5.5 OLED TV

OLED TV market has been dominated by LG, which opted for the bottom-emission [WOLED + CF] (RGBW) technology [195] coupled with a transparent *a*-IGZO TFT backplane to realize its UHD full-color TV (the latest addition is the 88-in 8K OLED TV). The advantage of this technology is that its fabrication did away with the troublesome FMM, which has often been one of the main causes for low yield in large-sized OLED production. Besides, it also allows for scaling up to Gen 10.5, like those realized by the TFT-LCD industry. But, the disadvantage is that in this pixelation approach, the efficiency as well as a certain degree of resolution due to the color filtering effect of RGBW is compromised. Therefore, one must also maximize brightness, color gamut, and ensure the robustness of its WOLED backlight, which needs to be lit at very high brightness for a long

time. For that, LG Display [196] has specially developed a hybrid tandem three-stack three-color WOLED bottom-emission structure, which is composed of one fluorescent blue stack, one phosphorescent Y/G/R stack, and one additional fluorescent blue stack. They are serially connected by two CGLs in sequence and sandwiched between the transparent ITO anode and the reflective Al cathode. The phosphorescent red EML is inserted next to the Y/G EML in the second stack for the purpose of enhancing the red sub-pixel efficiency as well as its color coordinates to reach $CIE_{x,y}$ (0.678, 0.321), while the green is $CIE_{x,y}$ (0.279, 0.666). The new WOLED structure also needs a mixed host of *n*-type and *p*-type HTMs. By proper adjustment of the ratio of the host mixture to balance the YG and R EL, a cool white of 7600 K with $CIE_{x,y}$ (0.308, 0.315) and a high efficiency of 83 cd A^{-1} at 12 V is achieved.

While detailed product information is unavailable, it is likely that the new UHD OLED TV series recently launched by LG is based on this WOLED architecture and the much improved *a*-IGZO TFT technology. For the latter, LG has developed a highly reliable oxide TFT backplane ($\Delta V_{th} \sim 0.4$ V under prolonged PBTS) with an internal gate driver IC (GIP circuit) and a very short channel length ($L = 4.5\,\mu m$) suitable for narrow bezel applications [197]. In addition, advanced pixel structure [198] and external compensation technology [199] must also be applied to maintain the luminescence uniformity. Other value-added innovations LG has introduced to the large-sized premium OLED TV include the Crystal Sound exciter speaker system [200] to enhance HiFi sound quality and the high transmittance polarizer technology [201] with reversed quarter wave plate (r-QWP) to improve power consumption and the lifetime of OLED panels. Last, but certainly not the least, is the long-awaited LG Signature 65-in 4K flexible OLED rollable TV [202], whose screen can rise from and recess into a slot in its oblong base to be marketed in 2020 (Figure 1.17).

1.5.6 Transparent OLED

The concept of transparent OLED has been demonstrated back in early 2000, long before OLED smartphones became popular. But to date, few creditable transparent display products based on OLED technology are seen in the marketplace (even though Xiao Mi has just announced the introduction of a rather expensive 65″ transparent OLED TV as shown in Figure 1.17). Perhaps, the technology was not mature then, or the transparent OLED displays were just not much different from those of the other capable display technologies (like LCDs), thus few people can really appreciate their full potential. However, given time for further development, improvement, and continuing investment, it is likely that the dawn of the age of flexible OLED may just well change all that.

Today, it appears that the best application field for transparent OLED is in transportation, such as in automobile, where both transparency and information are important in a display. In 2020, the Display Application Award of SID was awarded to the Audi AG's 7-in OLED Virtual Mirror System [192], which was debuted in Audi's all-electric car *e-tron* currently available in Europe. A camera is integrated into the hexagonal end of the virtual mirror's flat supports, and its images are digitally processed and displayed on the high-contrast, 1280 × 800-pixel OLED displays in the transition between the instrument panel and the door. In early test drives, it was realized that due to the superb *black* and the temperature-independent fast switching time, the transparent OLED had to be the best solution for this application.

Another eye-catching example is the 55-in transparent AMOLED made by LG, recently installed on the windows of the Beijing and Shenzhen (China) Metro subway trains. This "Magic Window" (as it is better known by the passengers) is capable of displaying all of the information related to the subway transit in high contrast, with fast response and full-color video images without blocking any view from the outside. It is reported that the transparency of this OLED display is about

40%, which is fabricated on the *a*-IGZO TFT backplane [139] using LG's [WOLED + CF] technology. The surface reflectivity of transparent OLED can be significantly reduced (to 6.5%) by laminating an anti-reflectance (AR) film on top of the CF substrate [203].

1.5.7 OLED Micro-Displays

According to International Data Corporation's 2018 forecast, the total number of shipped augmented reality (AR) and virtual reality (VR) headsets will grow to about 70 million units in 2022 and 100 million in 2025. Many experts believe that OLED micro-display, which is a special kind of OLED displays fabricated on a single crystal silicon (CMOS) backplane, is the best for VR displays [204]. This is because OLED, with its unsurpassed deep black, fast response time, lightweight, and thin, small form factor, can offer true immersive VR experience and ergonomic set design much better than LCD in a head-mount display (HMD). One of the major problems in VR displays is its motion blur, which is the after-image of a moving object in a still background scene during eye tracking. To reduce motion blur, black insertion methodology, which turns sample-and-hold type of driving into one of impulse-like by reducing persistence time, is often used in industry. However, the black insertion method at 60 Hz frame rate could cause serious flicker problem in LCD due to its slow response time. Therefore, OLED with its advantage of extremely fast response time that can be driven at higher frame frequency (>90 Hz) to remove flicker and further reduce motion blur is best for VR application [205]. Currently, many major VR HMD makers, such as HTC, Oculus, and Sony, consider OLED micro-display as a de facto standard, which has been chosen for their stand-alone VR sets introduced in the marketplace.

For AR application, which is big in the military, the OLED advantage is not all that obvious. Although an 18-megapixel 4.3″, 1443 ppi, 120 Hz display on glass for a wide field of view with high acuity HMD has been demonstrated [206], which adopted a [WOLED + CF] structure for high-density pixelation and an *n*-type LTPS backplane for faster response time. This is because in AR, where the image is projected against the real-world environment, high brightness ($>2000\,cd\,m^{-2}$) is necessary to render data or images that can be viewed in ambient lighting or when used with inefficient lenses or waveguides [207]. It is also important to have a high contrast ratio so that the projected display area does not glow and become washed out relative to the surroundings.

Although OLED micro-displays are capable of generating high-quality, high-resolution images that meet many of the requirements of VR/AR applications, the maximum luminance of conventional full-color OLED based on [WOLED + CF] technology remains well below the $2000\,cd\,m^{-2}$ minimum threshold requirement of VR/AR. The luminance of this kind of top-emission device structure is reduced drastically by up to 80% after TFE. Eliminating the color filters and directly patterning individual SBS RGB OLED emitters offers significant improvements in efficiency and luminance. However, the small sub-pixel size (typically less than $3 \times 10\,\mu m$) presents a major technological challenge as the patterned dimensions are well below that normally achievable by standard FMM.

But, these issues may have been resolved by the recent announcement of eMagin [208], which demonstrated a directly patterned (DP) RGB OLED micro-display on a Si backplane without the use of a metal mask, reaching exceptionally high luminance of $>7000\,cd\,m^{-2}$ with a resolution of 1920×1200 (2K×2K) and a sub-pixel size as small as $2.45 \times 8.85\,\mu m$. While detailed patterning methodology is not disclosed at press time, it is to be expected that by working on improving the technology and manufacturing process, the AR/VR market based on OLED through business and investment support will soon take off.

1.5.8 OLED Lightings

Lighting application could be the final frontier for OLED to conquer [209]. Much research has been devoted to the development of WOLED as one of the most comfortable, environmentally friendly, and healthiest solid-state lightings (SSL). It is thin and light, capable of delivering warm, homogeneous, large-area illumination without any blue light hazard [210] (BLH). In addition, OLEDs possess novel features such as transparency and flexibility, which will further increase their marketability and provide a much greater differentiation from current technology of LED. Figure 1.17 shows some of the notable examples and uses of OLED lighting, including innovative and flexible OLED lighting from Konica Minolta and LG Display, OLED lighting glass panels from OLED Works, luminaires from Acuity Brands, and tail lighting for automobiles from BMW and Audi.

1.5.8.1 General Lighting

The lighting industry is in rapid transition, from early inefficient incandescent lamps to long fluorescent tubes and environmentally unsafe compact fluorescent lamps, which are being replaced by SSL. The dominant solid-state technology is LED lighting, and their costs have been reduced drastically while their performance surpasses any other lighting technology. This situation is becoming rather difficult for OLED because most commercially available OLED lighting panels of today can only achieve up to about 60–85 lm W^{-1} at a luminance of 1000–3000 cd m^{-2} and a CCT of <3000 K. However, being an area source of lighting devoid of glare, OLED has a distinct advantage over LED, which relies on a bright point source. This is because OLED doesn't need any diffuser and heat sink, which adds cost, bulk, and weight, and decreases lighting efficiency. As a result, the OLED lighting panel is essentially a stand-alone luminaire that allows light to be brought close to the user, thus providing much higher system lighting application efficiencies [194].

The US Department of Energy (DOE) in Jan/2020 has published a roadmap for OLED lighting opportunities in which the target panel efficacy is projected to reach 155 lmW^{-1} by 2025 (Table 1.4) [211]. Another area of major challenge that OLED lighting must face is the cost. Although there were a few Co's that have gone into mass production of OLED lighting, current panel costs are still in the range of 1000–2000 $\$m^{-2}$, which is too high for the long-term goal of OLED lighting. In order to enable high-volume sales in competition with LED, the manufacturing cost of OLED lighting panels needs to be reduced to about 200 $\$m^{-2}$, which will then allow luminaires to be sold in the acceptable range of 400–600 $\$m^{-2}$. So, there is still much work to be done, and major challenges remain for OLED lighting to be competitive in indoor lighting applications.

Table 1.4 Projections (2019) by the US DOE showing roadmap for OLED efficiencies.

Metric	2019	2022	2025	2035
Panel efficacy (lm/W)	85	120	155	180
Optical efficiency of luminaire	100%	100%	90%[†]	90%[†]
Efficiency of driver	88%	90%	92%	95%
Total efficiency from device to luminaire	88%	90%	81%	86%
Resulting luminaire efficacy[*] (lm/W)	72	108	128	154

Source: [211] / U.S. Department of Energy / public domain.
[*] Efficacy projections assume CRI > 90, CCT 3000 K.
[†] Losses representing possible use of beam shaping optics.

Most of the efficiency advances are expected to be driven primarily by improvements in out-coupling efficiency, which relates to the amount of light emitted by an OLED device relative to that generated internally. These losses occur as photons are trapped in the substrate due to total internal reflection (TIR) at the glass–air interface and are guided within the organic material layers and the transparent anode due to their high refractive indices compared to that of glass. Photons are also dissipated at the organic/cathode interface by exciting surface plasmon polariton modes. This leads to an EQE of only about 20%, with an anisotropic distribution of emitter sites (see Section 1.2.1.4) on conventional glass substrates without out-coupling enhancements. Various methods involving internal enhancement structure (IES) [212] and external enhancement structures [213] (EES), like micro-lens array [214, 215], light-scattering layer [216], and high refractive index substrate [217], have been reported to reduce the above losses. High-efficiency OCEANCLEAR® IES substrates, which are made of high refractive index nanocrystals and heat-resisting carrier resin, have actually been applied to a Gen-II line for mass production at First-O-Lite, Inc. of China [218]. White OLED panels made on IES substrates have been shown to achieve a power efficacy of around 95 lm W^{-1} at 1000 cd m^{-2}.

For the record, LG Display is the first Co. that began mass production in the Gen-5 OLED lighting factory [219, 220] in late 2017. OLED Works is the other who in 2018 claimed to have produced the Brite3 family of OLED lighting panels [221] on a glass substrate with an efficacy of 80–90 lm W^{-1}, CRI > 90, and an LT70 lifetime > 30 000 hours at high brightness of (3000 cd m^{-2}). With an emitting area of about 100 cm^2, the panels operated at over 8000 cd m^{-2} are capable of producing 300 lumens per panel. This high performance is made possible by using both IES and EES light extraction technology along with optimization of the tandem OLED stack and the introduction of a highly reflective silver cathode. They also introduced a high-efficiency 50–60 lm W^{-1} (without IES) bendable OLED lighting panel constructed on 100 μm UTG provided by Corning.

One of the highest efficiency flexible WOLED lighting panels [222] was reported by SEL of Japan, who achieved about 110 lm W^{-1} by sandwiching an OLED between an out-coupling film and a SSF. The out-coupling film, which was used directly as a substrate (360 × 300 mm), was made of transparent plastic with a high refractive index (e.g. polyester-based plastic). With this material, TIR at the interface between the anode, the passivation film, and the substrate can be suppressed. The WOLED was fabricated on a glass support and then transferred to the plastic substrate using the matured transfer technology of AMOLED. Molybdenum oxide (MoO_x) was used as a *p*-dopant in HTL, while highly efficient and stable blue fluorescent, green, and orange phosphorescent materials were used as emitters, and silver was used as a reflective cathode. The color temperature of this large, flexible WOLED panel was 2860 K at 1000 cd m^{-2} and 3.23 V with a $CIE_{x,y}$ (0.49, 0.50). Although it was claimed that the projected LT50 was about 300 000 hours for a small test sample device of 4 mm^2, the LT of the large flexible WOLED lighting panel, along with its reliability and manufacturability, is yet unproven and remains questionable.

1.5.8.2 Automotive Lighting

While WOLED lighting production is still in its infancy today, many experts in the field believe the first "killer application" for OLED lighting could be for automobiles [223]; hence begin to change their R&D focus and market strategy. For instance, German carmaker BMW launched the first M4 GTS model vehicle using Osram's OLED panels in 2015, Audi unveiled its new TTRS and A8 [224] with segmented OLED taillights in 2016, and Benz S-Class model car did the same in 2017. In general, automobile lamp can be differentiated into illumination and signal indicator light by functionality or indoor and outdoor lights by its placement. Different positions of lamps may require

different color chromaticity, luminous flux, temperature tolerance, and lifetime, along with various degree of difficulties.

Other than the OLED displays installed inside the vehicle, by far, the most pursued area of OLED lighting application in automobile is the segmented taillights [225]. State-of-the-art OLED light engines need to achieve 2000 cd m^{-2} at deep red color coordinates of 1931 $CIE_{x,y}$ (0.3, 0.7) or even darker, which presents a major challenge for the development of deep red phosphorescent material. Achieving such a deep red emitter requires a peak ELwavelength (λ_{max}) above 630 nm and a very high degree of spectral purity. To reach this target performance, UDC has recently reported [226] a bottom-emission OLED that produced EL $\lambda_{max} = 640$ nm with an narrow FWHM = 43 nm and a lifetime of LT95 = 55 000 hours at an initial luminance of 1000 cd m^{-2}. Lighting outside the vehicle body needs to also tolerate extreme temperature, which could get hotter than 85 °C (even up to 120 °C) because of the sunlight radiation and closed lamp design. There are other challenges for OLED lighting application in automobile such as reliability and cost that must be met before it can be competitive in the marketplace [227].

Finally, it is important to point out that to date all mass-produced OLED tail lamps utilize planar glass substrates, which greatly limit the degrees of freedom in integrating the two-dimensional OLED panels into a three-dimensional curved lamp design to wrap around the tail end of a car. For this, flexible OLEDs are needed and must be adapted for use in automotive lighting applications in the future.

1.6 Summary and Outlook

It is impossible to introduce fundamentals of OLED in any breadth or depth in these pages due to the limitation of space. Interested readers are encouraged to read further with the extensive list of references cited and the ensuing chapters written by many experts in their respective fields.

It suffices to state that the future of OLEDs as displays and lighting is extremely bright and colorful, which presents great opportunities for numerous inventions and innovations in research and development as the technology matures and improves over time. We will witness the explosive growth of OLED investment and business as mass production of flexible OLEDs is under way both in Korea and in China. It took nearly 40 years to advance OLED from merely a laboratory curiosity in Kodak to the Dream Display – AMOLED [33] of today – used in many of the top-line smartphones in the CE market. But, the OLED technology is far from perfect, and much work and many challenges remain, such as the efficiency and lifetime of deep blue materials, TFE, RGB pixelation, and cost reduction (e.g. developing IJP-printed OLED technology), just to name a few.

There are a number of emerging technologies like Micro LED, QD-OLED, and QLED that could present serious competition for OLED in the near future. Nevertheless, it is all but certain that the killer application of OLED is flexible display, and it will take all of us working together in this exciting field of OLED to realize that dream.

Acknowledgment

I would like to thank all my former students and close associates at National Chiao Tung Univ. (Taiwan), Hong Kong Baptist Univ., and Shanghai Jiao Tong Univ., and my fellow colleagues and friends at Kodak, *e*-Ray Optoelectronics, Junsun Technology, Shine Materials Technology of Taiwan, Aglaia (China), Shanghai Taoe Chemicals, and Wuhan Sun Shine Optoelectronics for

their contributions and support in advancing and promoting OLED technology and business across the strait of Greater China.

References

1 T. Tsujimura (2017). *OLED Display Fundamentals and Applications*, 2e. Hoboken, NJ: John Wiley & Sons, Inc.

2 M. Pope, H.P. Kallman, P. Magnante. Electroluminescence in organic crystals. *J. Chem. Phys*. **1963**, *38*, 2042–2043.

3 P.S. Vincett, W.A. Barlow, R.A. Hann, G.G. Roberts. Electrical conduction and low voltage blue electroluminescence in vacuum-deposited organic films. *Thin Solid Films*. **1982**, *94*, 171–183.

4 J. Kalinowski, J. Godlewski, Z. Dreger. High-field recombination electroluminescence in vacuum-deposited anthracene and doped anthracene films. *Appl. Phys. A: Mater. Sci. Process*. **1985**, *37*, 179–186.

5 C.W. Tang, S.A. VanSlyke. Organic electroluminescence diodes. *Appl. Phys. Lett*. **1987**, *51*, 913.

6 C.W. Tang, S.A. VanSlyke, C.H. Chen. Electroluminescence doped organic thin films. *J. Appl. Phys*. **1989**, *65*, 3610–3616.

7 For earlier reviews, see: J. Liu, C.-T. Chen, C.H. Chen (2015). Introduction to organic light-emitting diode (OLED). In: *The Handbook of Digital Imaging* (ed. M. Kriss), Chapter 14. New York: John Wiley & Sons, Ltd. 577–626.

8 J.H. Burroughes, D.D.C. Bradley, A.R. Brown, R.N. Marks, K. Mackay, R.H. Friend, P.L. Burns, A.B. Holmes. Light-emitting diodes based on conjugated polymers. *Nature*. **1990**, *347*, 539–541.

9 M.A. Baldo, D.F. O'Brien, Y. You, A. Shoustikov, S. Sibley, M. Thompson. Highly efficient phosphorescent emission from organic electroluminescence devices. *Nature*. **1998**, *395*, 151.

10 A. Tsuboyama, H. Iwawaki, M. Furugori. Homoleptic cyclometalated iridium complexes with highly efficient red phosphorescence and application to organic light-emitting diode. *J. Am. Chem. Soc*. **2003**, *125*, 12971–12979.

11 P.K. Raychaudhuri, J.K. Madathil, J.D. Shore, S.A. Van Slyke. Performance enhancement of top- and bottom- emitting organic light-emitting devices using microcavity structures. *J. Soc. Inf. Disp*. **2004**, *12*, 315–321.

12 K. Walzer, B. Maennig, M. Pfeiffer, Leo, K. Highly efficient organic devices based on electrically doped transport layers. *Chem. Rev*. **2007**, *107*, 1233–1271.

13 J. Kido, T. Matsumoto, T. Nakada, J. Endo, K. Mori, N. Kawamura, A. Yokoi (2003). High efficiency organic EL devices having charge generation layers. In: *SID Symposium Digest of Technical Papers*. Baltimore, MD. 964.

14 K.-H. Kim, C.-K. Moon, J.-H. Lee, S.Y. Kim, J.J. Kim. Highly efficient OLED with phosphorescent emitters having high quantum yield and horizontal orientation of transition dipole moment. *Adv. Mater*. **2014**, *26*, 3844.

15 H. Kuma, C. Hosokawa. Blue fluorescent OLED materials and their application for high performance devices. *Sci. Technol. Adv. Mater*. **2014**, *15*, 034201.

16 D. Volz. Thermally activated delayed fluorescence is a key new technology for OLED displays. *Inf. Displ*. **2017**, *33* (*2*), 16.

17 S. Tominetti, J. Gigli, S.H. Shih, Y.T. Su, J.H. Jou (2018). Seal encapsulation: OLED sealing processes. In: *Handbook of Organic Light-Emitting Diodes* (eds. C. Adachi, R. Hattori, H. Kaji et al.). Tokyo: Springer.

18 W. Brütting, S. Berleb, A.G. Mückl. Device physics of organic light-emitting diodes based on molecular materials. *Org. Electron*. **2001**, *2*, 1–36.

19 T. Tsutsui, K. Yamamato. Evaluation of true power luminous efficiency from experimental luminance values. *Jpn. J. Appl. Phys. Part 1*. **1999**, *38*, 2799.

20 W.J. Smith (2000). *Modern Optical Engineering*. New York, NY: McGraw-Hill. 221–222.

21 S.R. Forrest, D.D.C. Bradley, M.E. Thompson. Measuring the efficiency of organic light-emitting devices. *Adv. Mater*. **2003**, *15*, 1043–1048.

22 I. Tanaka, S. Tokito. Precise measurement of external quantum efficiency of organic light-emitting devices. *Jpn. J. Appl. Phys*. **2004**, 43, 7733.

23 T. Komoda, K. Yamae, V. Kittichungchit, H. Tsuji, N. Ide (2012). Extremely high performance white OLEDS for lighting. In: *SID Symposium Digest of Technical Papers*. Boston, MA: Blackwell Publishing Ltd. 610–613.

24 C.-C. Liu, S.-H. Liu, K.-C. Tien, M.H. Hsu, H.W. Chang, C.K. Chang, C.J. Yang, C.C. Wu. Electromagnetic modeling of OLED and its outcoupling efficiency. *Appl. Phys. Lett*. **2009**, *94*, 103302.

25 Y.S. Tyan, Y.X. Shen, J.J. Peng. Efficient tandem hybrid white OLEDs for solid state lighting application. *Digest Symp. SID*. **2014**, *47*, 675–678.

26 C.H. Chen, S.-W. Wen, C.-T. Chen (2018). Organic light-emitting diode (OLED). In: *Encyclopedia of Modern Optics*, 2e (eds. B. Guenther, D. Steel). UK: Academic Press, Elsevier Ltd. *3*, 64–69.

27 N. Elgrishi, K.J. Rountree, B.D. McCarthy, E.S. Rountree, T.T. Eisenhart, J.L. Dempsey. A practical beginner's guide to cyclic voltammetry. *J. Chem. Educ*. **2018**, *95* (*2*), 197–206.

28 J. Sworakowski. How accurate are energies of HOMO and LUMO levels in small-molecule organic semiconductors determined from cyclic voltammetry or optical spectroscopy. *Synth. Met*. **2018**, *235*, 125–130.

29 R. Holze. Optical and electrochemical bandgaps in mono-, oligo-, and polymeric systems: a critical reassessment. *Organometallics*. **2014**, *33* (*18*), 5033–5042.

30 I.G. Hill, A. Kahn, Z.G. Soos, R.A. Pascal Jr. *Chem. Phys. Lett*. **2000**, *327*, 181–188.

31 S. Barth, U. Wolf, H. Bässler, P. Müller, H. Riel, H. Vestweber, P.F. Seidler, W. Riess. *Phys. Rev. B*. **1999**, *60*, 8791.

32 M.A. Lambert, P. Mark. (1970). *Current Injection in Solids*. New York, NY: Academic Press. 558.

33 C.H. Chen, S.-W. Huang (2007). *OLED: Materials and Devices of a Dream Display*. Taipei, Taiwan: Wunan Publishing Co. http://www.wunan.com.tw.

34 W.D. Gill. J. Appl. *Phys*. **1972**, *43*, 5033.

35 S.K. So, S.C. Tse, H.H. Fong, C.H. Chen (2005). Charge conduction in fused aromatic compounds for OLEDs applications. In: *Proceedings of IDMC*. Taipei, Taiwan. 275–277.

36 A. Kumar, H.-H. Liao, Y. Yang. Hole mobility in optimized organic photovoltaic blend films obtained using extraction current transients. *Org. Electron*. **2009**, *10*, 1615–1620.

37 S.W. Tsang, S.K. So. Advantages of admittance spectroscopy over time-of-flight technique for studying dispersive charge transport in an organic semiconductor. *J. Appl. Phys*. **2009**, *106*, 083710.

38 B.M. Krasovitskii, B.M. Bolotin (1988). Organic luminescent materials (ed. V G. Transl. by Vopian). Weinheim, Federal Republic of Germany: VCH.

39 W.D. Wright. Experimental origins of the 1931 CIE system of colorimetry. *J. Coat. Tech*. **1982**, *54* (*685*), 65.

40 Y. Shirota, H. Kageyama. Charge carrier transporting molecular materials and their applications in devices. *Chem. Rev*. **2007**, *107*, 953.

41 Commission Internationale de l'Eclairage (CIE), Publication No. 15.2 (1986), *Colorimetry*, 2e. CIE, Vienna.

42 A. Sharma. Understanding RGB color spaces for monitors, projectors and television. *Inf. Disp*. **2019**, *2*, 17.

43 Recommendation ITU-R BT.2020-2, Parameter values for ultra-high definition television systems for production and international programme exchange, International Telecommunication Union (2015). https://www.itu.int/rec/R-REC-BT.2020-2-201510-I/en.

44 C. Féry, B. Racine, D. Vaufrey, H. Doyeux, S. Cinà. Physical mechanism responsible for the stretched exponential decay behavior of aging organic light-emitting diodes. *Appl. Phys. Lett*. **2005**, *87* (*213502*), 1–3.

45 T. Yoshioka, K. Sugimoto, H. Ohata, S. Miyaguchi, T. Tsutsui. Comprehensive analysis of luminous decay curves for accelerated lifetime testing of OLEDs. *SID Symp. Digest Tech. Papers*. **2015**, *46* (*1*), 1650.

46 T. Yoshioka, K. Sugimoto, K. Katagi, Y. Kitago, M. Tajima, S. Miyaguchi, T. Tsutsui, R. Iwasaki, Y. Furukawa. An improved method for lifetime prediction based on decoupling of the joule self-heating effect from coulombic degradation in accelerated aging tests of OLEDs. *SID Symp. Digest Tech. Papers*. **2014**, *45* (*1*), 642–645.

47 S. Garner, G. Merz, G.S. Glaesemann, J. Tosch, C. Chang, D. Marshall, X. Li, L. Tian, K. Vasilakos, A. Gagov. Ultra-slim flexible glass substrate for display applications. *SID Symp. Digest Tech. Papers*. **2012**, *43* (*1*), 342.

48 T. Furukawa, K. Mitsugi, S. Akiyama, H. Itoh, D. Kobayashi, T. Suzuki, H. Kuroiwa, M. Sakakibara, K. Tanaka, N. Kawamura, M. Koden (2014). ITO pattern formed by roll-to-roll process on ultra-thin glass. In: *Proc. IDW'14, Japan*, FLX3-4L, 1428–1429.

49 T. Furukawa, M. Koden. Novel R2R and printing technologies for electrodes of flexible OLED lighting. *Int. Conf. Disp. Technol.* (*ICDT*). **2019**, *50* (*S1*), 595–598.

50 M. Junghähnel, S. Weller, T. Gebel. Advanced processing of ITO and IZO thin films on flexible glass. *SID Symp. Digest Tech. Papers*. **2015**, *46* (*1*), 1378–1381.

51 N. Yamada, T. Ogura, Y. Kubo. Evaluation of electrical insulating properties and flexibility of stainless steel foil with insulating films. *SID Symp. Digest Tech. Papers*. **2008**, *39* (*1*), 136–139.

52 N. Yamada, S. Yamaguchi, J. Nakatsuka, Y. Hagiwara, K. Uemura. Planarized stainless steel foil for flexible substrate. In: *Proc. IDW'15 Japan*. **2015**, FMC3-1.

53 WA. MacDonald, K. Rolins, D. MacKerran, R. Eveson, R.A. Rustin, K. Rakos, M. Handa. Plastic displays – latest developments in polyester film for plastic electronics. *SID Symp. Digest Tech. Papers*. **2004**, *35* (*1*), 420.

54 L. Bu, L. Carbajal, M. Chang, J. Chen, J.C. Johnson, K. Kourtakis, M. Lamontia, A. Li, K. Liao, S. Liu, M. Mulzer. Advanced materials for flexible displays. *SID Symp. Digest Tech. Papers*. **2019**, *50* (*1*), 727–730.

55 T. Sashimo, K. Noda, J. Hikida. et al. Coating materials technology for flexible OLED display. *SID Symp. Digest Tech. Papers*. **2018**, *49* (*1*), 333.

56 H.F. Xie, Y. Shi, M.C. Lu, N. Liu, Z.H. Li, L. Wen, X.R. Mei, S.J. Chen, S.D. Zhang, C.Y. Lee. Effect of buffer layer on performance and reliability of flexible a-IGZO TFTs fabricated on colorless polyimide of G4.5. *SID Symp. Digest Tech. Papers*. **2019**, *50* (*1*), 1218–1221.

57 M.-F. Chiang, C.-C. Cheng, C.-H. Tu, C.Y. Liu, T.H. Huang, J.K. Lu, N. Sugiura, Y.C. Lin. Handling technology of plastic substrates in flexible display manufacturing. *SID Symp. Digest Tech. Papers*. **2014**, *45* (*1*), 46–49.

58 AT. Huang, C.-S. Chan, C.-L. Wang, C.C. Chang, Y.H. Lai, C.H. Tu, M.T. Lee. Flexible AMOLED display make progress. *Inf. Disp*. **2016**, *32* (*2*), 18.

59 C.C. Wu, C.I. Wu, J.C. Sturm, A. Kahn. Surface modification of indium tin oxide by plasma treatment: an effective method to improve the efficiency, brightness, and reliability of organic light emitting devices. *Appl. Phys. Lett*. **1997**, *70*, 1348–1350.

60 J.-H. Jung, S.-J. Lee, H.S. Hwang, H.K. Baik, N.I. Cho. Fabrication of IZO transparent conducting thin films by the use of magnetron sputtering equipped with ion-beam system. *J. Soc. Inf. Disp*. **2009**, *17* (*9*), 745–750.

61 D.J. Lee, Y.W. Park, B.-K. Ju. Ultra-smooth silver nanowires flexible transparent electrode for organic light emitting diodes. *SID Symp. Digest Tech. Papers*. **2018**, *49* (*2*), 1859–1861.

62 S. Chen. Recent developments in top-emitting organic light-emitting diodes. *Adv. Mater*. **2010**, *22*, 5227–5239.

63 J. Springer. Absorption loss at nano-rough silver back reflector of thin-film silicon solar cells. *J. Appl. Phys*. **2004**, *95*, 1427–1429.

64 M. Stössel, J. Staudigel, F. Steuber, J. Simmerer, A. Winnacker. Impact of the cathode metal work function on the performance of vacuum-deposited organic light emitting-devices. *Appl. Phys. A*. **1999**, *68*, 387–390.

65 H. Heil, J. Steiger, S. Karg, M. Gastel, H. Ortner, H. Von Seggern, M. Stößel. Mechanisms of injection enhancement in organic light-emitting diodes through an Al/LiF electrode. *J. Appl. Phys*. **2001**, *89*, 420–424.

66 P.E. Burrows. Control of microcavity effect in full color stacked organic light emitting devices. *Appl. Phys. Lett*. **1998**, *73*, 435–437.

67 J. Cao. RGB tricolor produced by white-based top-emitting organic light-emitting diodes with microcavity structure, *Curr. Appl. Phys*. **2007**, *7*, 300–304.

68 S.K. Kim, H.I. Yang, R. Lampande, J.H. Kwon. High efficiency top-emission organic light emitting diodes realized using newly developed low absorption pure Ag cathode configuration. *SID Symp. Digest Tech. Papers*. **2019**, 50 (1), 50–53.

69 B. Caron, T. Maindron, B. Racine, S. Meunier-Della-Gatta, N. Vaxelaire, E. Quesnel. Ag:WO_3 cement as a stable cathode with low and tunable reflectance for top-emission OLED. *SID Symp. Digest Tech. Papers*. **2019**, *50* (*2*), 1920–1923.

70 Z.B. Deng, X.M. Ding, S.T. Lee, W.A. Gambling. Enhanced brightness and efficiency in organic electroluminescent devices using SiO_2 buffer layers. *Appl. Phys. Lett*. **1999**, *74*, 2227–2229.

71 Y. Shirota, Y. Kuwabara, H. Inada, T. Wakimoto, H. Nakada, Y. Yonemoto, S. Kawami, K. Imai. Multilayered organic electroluminescent device using a novel starburst molecule, 4,4',4''-tris(3-methylphenylphenylamino)triphenylamine, as a hole transport material. *Appl. Phys. Lett*. **1994**, *65*, 807–809.

72 G.F. He, M. Pfeiffer, K. Leo, M. Hofmann, J. Birnstock, R. Pudzich, J. Salbeck. High-efficiency and low-voltage p-i-n electrophosphorescent organic light-emitting diodes with double-emission layers. *Appl. Phys. Lett*. **2004**, *85*, 3911–3913.

73 J. Meyer, T. Winkler, S. Hamwi, S. Schmale, H.H. Johannes, T. Weimann, P. Hinze, W. Kowalsky, T. Riedl. Transparent inverted organic light-emitting diodes with a tungsten oxide buffer layer. *Adv. Mater*. **2008**, *20*, 3839–3843.

74 J.W. Ma, Z. Liang, C. Jin, X.Y. Jiang, Z.L. Zhang. Enhanced power efficiency for white OLED with MoO_3 as hole injection layer and optimized charge balance. *Solid State Comm*. **2009**, *149*, 214–217.

75 D.B. Romero, M. Schaer, L. Zuppiroli, B. Cesar, B. Francois. Effects of doping polymer light-emitting diodes. *Appl. Phys. Lett*. **1995**, *67*, 1659–1661.

76 J. Blochwitz, M. Pfeiffer, T. Fritz, K. Leo. Low voltage organic light emitting diodes featuring doped phthalocyanine as hole transport material. *Appl. Phys. Lett*. **1998**, *73*, 729–731.

77 S.-H. Son, J.-G. Jang, S.-Y. Jeon. et al. (2004). *WO 2004054326*.

78 O. Zelka, S. Willmann, A. Lux, H. Hartmann, S. Dorok, A. Werner (2010). Radialene compounds and their use. *US2010/0102709 A1*.

79 S.A. VanSlyke, C.H. Chen, C.W. Tang. Organic electroluminescent devices with improved stability. *Appl. Phys. Lett*. **1996**, *69*, 2160–2162.

80 Y. Shirota, K. Okumoto, H. Inada. Thermally stable organic light-emitting diodes using new families of hole-transporting amorphous molecular materials. *Synth. Met*. **2000**, *111*, 387–391.

81 U. Mitschke, P. Bäuerle. The electroluminescence of organic materials. *J. Mater. Chem*. **2000**, *10*, 1471–1507.

82 M.-H. Ho, B. Banumurthy, C.H. Chen. Blue fluorescence and bipolar transport materials based on anthracene and their applications in OLEDs. *Israel J. Chem*. **2012**, *52*, 484–495.

83 S.C. Tse, S.K. So, M.Y. Yeung, C.F. Lo, S.W. Wen, C.H. Chen. The role of charge-transfer integral in determining and engineering the carrier mobilities of 9, 10-di (2-naphthyl) anthracene compounds. *Chem. Phys. Lett*. **2006**, *422*, 354–357.

84 H. Fujikawa, T. Mori, K. Noda, M. Ishii, S. Tokito, Y. Taga. Organic electroluminescent devices using alkaline-earth fluorides as an electron injection layer. *J. Lumin*. **2000**, *87*, 1177–1179.

85 M.-T. Hsieh, M.-H. Ho, K.-H. Lin, J.F. Chen, T.M. Chen, C.H. Chen. Study of electric characteristics and diffusion effects of 2-methyl-9,10-di(2-naphthyl)anthracene doped with cesium fluoride by admittance spectroscopy. *Appl. Phys. Lett*. **2010**, *96*, 133310.

86 Y. Lee, J. Kim, S. Kwon, C.K. Min, Y. Yi, J.W. Kim, B. Koo, M. Hong. Interface studies of aluminum, 8-(hydroxyquinolato)lithium (Liq) and Alq_3 for inverted OLED application. *Org. Electron*. **2008**, *9*, 407–412.

87 M. Stößel, J. Staudigel, F. Steuber, J. Blässing, J. Simmerer, A. Winnacker. Space-charge-limited electron currents in 8-hydroxyquinoline aluminum. *Appl. Phys. Lett*. **2000**, *76*, 115–117.

88 K. Walzer, B. Maennig, M. Pfeiffer, K. Leo. Highly efficient organic devices based on electrically doped transport layers. *Chem. Rev*. **2007**, *107*, 1233–1271.

89 J. Kido, T. Matsumoto. Bright organic electroluminescent devices having a metal-doped electron-injecting layer. *Appl. Phys. Lett*. **1998**, *73*, 2866–2868.

90 X.L. Zhu, J.X. Sun, X.M. Yu, M. Wong, H.S. Kwok. Very bright and efficient top-emitting OLED with Yb as effective electron injector. *SID Symp. Digest Tech. Papers*. **2012**, *37* (*1*), 1292–1295.

91 S.-J. Su, Y. Takahashi, T. Chiba, T. Takeda, J. Kido. Structure-property relationship of pyridine-containing triphenyl benzene electron-transport materials for highly efficient blue phosphorescent OLEDs. *Adv. Funct. Mater*. **2009**, *19*, 1260–1267.

92 V.I. Adamovich, S.R. Cordero, P.I. Djurovich, A. Tamayo, M.E. Thompson, B.W. D'Andrade, S.R. Forrest. New charge-carrier blocking materials for high efficiency OLEDs. *Org. Electron*. **2003**, *4*, 77–87.

93 H.-Y. Jang, J.-C. Lee, J.-S. Bae, J.-G. Kim, S.-S. Kim, C.-H. Kim (2012). *US20120037892 A1*.

94 C.H. Kim (2017). *Organic Light-Emitting Compound and Organic Luminescent Element using Same*. *WO2017/179809A1*.

95 K. Yamaguchi, T. Matsushima, A.S.D. Sandanayago, Y. Homma, N. Uchida, C. Adachi. Enhanced operational durability of thermally activated delayed fluorescence-based OLEDs with a triazine electron transporter. *Chem.-A Eur. J*. **2020**, *26* (*25*), 5598–5602.

96 H. Sasabe, R. Sato, K. Suzuki, Y. Watanabe, C. Adachi, H. Kaji, J. Kido. Ultrahigh power efficiency of thermally activated delayed fluorescent OLEDs by the strategic use of electron-transport materials. *Adv. Opt. Mater*. **2018**. *6* (*17*), 1800376.

97 W.-Y. Wong. Special issue: OLED materials and devices. *Chem. Rec*. **2019**, *19* (*8*), 1470.

98 S. Monima, K.-T. Wong. Development of materials for blue organic light emitting devices. *Chem. Rec*. **2019**, *19* (*10*), 1002.

99 M.L. Ricks, J.R. Vargas, K.P. Klubek, V.V. Jarikov, L.S. Liao, M.J. Helber, W.J. Begley, T.K. Hatwar, S.R. Conley, L. Cosimbescu, C.T. Brown. (2007). Efficient, long-lifetime OLED host and dopant formulations for full-color displays. In: *SID Symposium Digest of Technical Papers*. Long Beach, CA. *38*, 830–833.

100 S. Lamansky, P. Djurovich, D. Murphy, F. Abdel-Razzaq, R. Kwong, I. Tsyba, M. Bortz, B. Mui, R. Bau, M.E. Thompson. Synthesis and characterization of phosphorescent cyclometalated iridium complexes. *Inorg. Chem*. **2001**, *40*, 1704–1711.

101 S.R. Forrest. Excitons and lifetime of organic semiconductor devices. *Philos. Trans. A*. **2015**, *373*, 20140320.

102 H. Uoyama, K. Goushi, K. Shizu, H. Nomura, C. Adachi. Highly efficient organic light-emitting diodes from delayed fluorescence. *Nature*. **2012**, *492*, 234–238.

103 D. Zhang, L. Duan, D. Zhang, J. Qiao, G. Dong, L. Wang, Y. Qiu. Extremely low driving voltage electrophosphorescent green organic light-emitting diodes based on a host material with small singlet–triplet exchange energy without *p*- or *n*-doping layer. *Org. Electron*. **2013**, *14*, 260–266.

104 J. Adachi, H. Kakizoe, P.K.D. Tsang, A. Endo. Hyperfluorescence™; a game changing technology of OLED display. *Proc. Int. Conf. Disp. Technol. (ICDT)*. **2019**, *50*, 95–98.

105 Y. Pan, W. Li, S. Zhang, L. Yao, C. Gu, H. Xu, B. Yang, Y. Ma. High yields of singlet excitons of organic electroluminescence through two paths of cold and hot excitons. *Adv. Opt. Mater*. **2014**, *2*, 510–515.

106 Y. Xu, X. Liang, X. Zhou, P. Yuan, J. Zhou, C. Wang, B. Li, D. Hu, X. Qiao, X. Jiang, L. Liu. Highly efficient blue fluorescent OLEDs based on upper level triplet-singlet intersystem crossing. *Adv. Mater*. **2019**, *31*, 1807388.

107 Y. Xu, C. Wang, X. Zhou, J. Zhou, X. Guo, X. Liang, D. Hu, F. Li, D. Ma, Y. Ma. Fine modulation of the higher order excitonic states toward more efficient conversion from upper-level triplet to singlet. *J. Phys. Chem. Lett*. **2019**, *10*, 6878–6884.

108 S. Yamazaki, T. Tsutsui (2017). *Physics and Technology of Crystalline Oxide Semiconductor Caac-Igzo: Applications to Displays*. Chichester, UK: John Wiley.

109 N. Thompson (2018). Lighting our way with OLED advancements for displays and illumination. *Internat. Conf. Displ. Technol*. (*ICDT*), presentation by UDC, China: Guangzhou.

110 D. Zhang, L. Duan, Y. Li, H. Li, Z. Bin, D. Zhang, J. Qiao, G. Dong, L. Wang, Y. Qiu. Towards high efficiency and low roll-off orange electrophosphorescent devices by fine tuning singlet and triplet energies of bipolar hosts based on indolocarbazole/1,3,5-triazine hybrids. *Adv. Funct. Mater*. **2014**, *24*, 3551–3561.

111 D. Zhang, L. Duan, D. Zhang, Y. Qiu. Towards ideal electrophosphorescent devices with low dopant concentrations: the key role of triplet upconversion. *J. Mater. Chem. C*. **2014**, *2* (*42*), 8983–8989. doi: 10.1039/C4TC01757A.

112 M.T. Lee, Y.S. Wu, H.H. Chen, C.H. Tsai, C.H. Liao, C.H. Chen (2004). Efficient blue organic electroluminescent devices based on a stable blue host material. In: *SID Symposium Digest of Technical Papers*. Seattle, WA. *35*, 710–713.

113 D.Y. Kondakov. Characterization of triplet-triplet annihilation in organic light-emitting diodes based on anthracene derivatives. *J. Appl. Phys*. **2007**, *102*, 114504.

114 车淳旭, 朴上雨 et al. (2018). Sun Fine Chemicals Co., Korea. *CN107619402A*.

115 E.A. Margulies, P.-L.T. Budreault, V.I. Adamovich, B.D. Alleyne, M.S. Weaver, J.J. Brown. Narrow spectrum deep red emitters for OLED lighting and display. *SID Symp. Digest Tech. Papers*. **2019**, *50* (*1*), 911–913.

116 T. Yamaguchi, H. Inoue, H. Kido, T. Sasaki, N. Ohsawa, S. Seo, S. Yamazaki. High-temperature operational stability of deep red phosphorescent OLED with exciplex-forming host and guest materials. *SID Symp. Digest Tech. Papers*. **2019**, *50* (*1*), 558–561.

117 M.A. Baldo, S. Lamansky, P.E. Burrows, M. Thompson, S. Forrest. Very high-efficiency green organic light-emitting devices based on electrophosphorescence. *Appl. Phys. Lett*. **1999**, *75*, 4–6.

118 S. Lamansky, P. Djurovich, D. Murphy, F. Abdel-Razzaq, H.E. Lee, C. Adachi, P.E. Burrows, S.R. Forrest, M.E. Thompson. Highly phosphorescent bis-cyclometalated iridium complexes: synthesis, photophysical characterization, and use in organic light emitting diodes. *J. Am. Chem. Soc*. **2001**, *123*, 4304–4312.

119 N. Ohsawa, S. Mitsumori, T. Sasaki, H. Kido, T. Watabe, H. Inoue, S. Seo, S. Yamazaki. Long-life green phosphorescent OLED with light-emitting layer formed by two-source evaporation using host material with novel hetero fused ring. *SID Symp. Digest Tech. Papers*. **2019**, *50* (*2*), 1916–1919.

120 Y. Kijima, N. Asai, S.-I. Tamura. A blue organic light emitting diode. *Jpn. J. Appl. Phys*. **1999**, *38*, 5274.

121 S.-K. Kim, B. Yang, Y. Ma, J.H. Lee, J.W. Park. Exceedingly efficient deep-blue electroluminescence from new anthracenes obtained using rational molecular design. *J. Mater. Chem*. **2008**, *18*, 3376–3384.

122 H. Kuma, C. Hosokawa. Blue fluorescent OLED materials and their application for high-performance devices. *Sci. Technol. Adv. Mater*. **2014**, *15*, 034201.

123 B.-J. Kim, Y.-I. Park, D. Yokoyama, J. Park (2012). Dual efficiency enhancement by delayed fluorescence and dipole orientation in high-efficiency fluorescent OLEDs. In: *SID Symposium Digest of Technical Papers*. Boston, MA. 541–544.

124 H.Y. Oh, O. Kim. Advances in deep blue emitters for highly efficient and long life organic light-emitting diodes. *SID Symp. Digest Tech. Papers*. **2018**, *49* (*1*), 132–135.

125 C.C. Yeh, M.T. Lee, H.H. Chen, C.H. Chen (2004). High-performance blue OLEDs based on sterically hindered pyrene host material. In: *SID Symposium Digest of Technical Papers*. Seattle, WA. 788–792.

126 H. Jung, S. Kang, H. Lee, Y.J. Yu, J.H. Jeong, J. Song, Y. Jeon, J. Park. High efficiency and long lifetime of a fluorescent blue light emitter made of a pyrene core and optimized side groups. *ACS Appl. Mater. Interfaces*. **2018**, *10* (*36*), 30028.

127 Y. Takita, N. Hashimoto, K. Takeda, S. Nomura, T. Suzuki, H. Nakashima, S. Uesaka, S. Seo, S. Yamazaki. Highly efficient deep-blue fluorescent dopant for achieving low-power OLED display satisfying BT.2020 chromaticity. *SID Symp. Digest Tech. Papers*. **2018**, *49* (*1*), 138–141.

128 T. Hatakeyama, T. Ikuta, K. Shiren, S. Hashimoto, S. Nakatsuka, H. Hirai, K. Nakajima, J. Ni, M. Nakamura. Triplet-energy control of PAHs by heteroatom incorporation for development of efficient materials for PHOLEDs. *SID Symp. Digest Tech. Papers*. **2015**, *46* (*1*), 401–403.

129 K.H. Lee, J.Y. Lee, H.Y. Oh. Boron derivatives as deep blue fluorescent materials for high efficiency and long lifetime OLED. *SID Symp. Digest Tech. Papers*. **2019**, *50* (*1*), 1924–1927.

130 T. Hatakeyama, K. Shiren, K. Nakajima, S. Nomura, S. Nakatsuka, K. Kinoshita, J. Ni, Y. Ono, T. Ikuta. Ultrapure blue thermally activated delayed fluorescence molecules: efficient HOMO-LUMO separation by the multiple resonance effect. *Adv. Mater*. **2016**, *28*, 2777–2781.

131 Y. Kondo, K. Yoshiura, S. Kitera, H. Nishi, S. Oda, H. Gotoh, Y. Sasada, M. Yanai, T. Hatakeyama. Narrow band deep-blue organic light-emitting diode featuring an organoboron-based emitter. *Nat. Photonics*. **2019**, *13*, 678–682.

132 A. Xiao, D. Cui, J.H. Shin, X. Chen. Influence of laser sealing process on frit hermetical performance. *SID Symp. Digest Tech. Papers*. **2015**, *46* (*1*), 1375.

133 H. Lifka, H.A. Esch, J.J.W.M. Rosink. Thin film encapsulation of OLED displays with a NONON stack. *SID Symp. Digest Tech. Papers*. **2004**, *33 (1)*, 1384–1387.

134 J.D. Affinito, M.E. Gross, C.A. Coronado, G.L. Graff, I.N. Greenwell, P.M. Martin. Barix films for encapsulation. *Thin Solid Films*. **1996**, *63*, 290–291.

135 H. Nominanda, W. Wu, J.R. Chen, S.Y. Choi. Large area thin film encapsulation from bendable to rollable and foldable. *SID Symp. Digest Tech. Papers*. **2018**, *49* (*1*), 1103–1105.

136 W. Ao, C. Li, Y. Wang, X. Liu, X. Xin, F. Gao, C. Peng, J. Zhang. AMOLED encapsulation technology and prospect. *Int. Conf. Disp. Technol. (ICDT*). **2018**, *49* (*S1*), 734–736.

137 S.S. Kim, H.S. Kim, J.G. Lee, C.W. Seo. Ultra-high precision inkjet printing technology for display. *SID Symp. Digest Tech. Papers*. **2018**, *49* (*1*), 839–842.

138 G. Nisato, M. Kuilder, P. Bouten, L. Moro, O. Philips, N. Rutherford. Thin film encapsulation for OLEDs: evaluation of multi-layer barriers using the Ca test. *Proc. SID* 2003 Int. *Symp*. **2003**, *34*, 88.

139 C.I.I. Park, M. Seong, M.A. Kim, D. Kim, H. Jung, M. Cho, S.H. Lee, H. Lee, S. Min, J. Kim, M. Kim. World 1st large size 77-inch transparent flexible OLED display. *SID Symp. Digest Tech. Papers*. **2018**, *49* (*1*), 710–713.

140 E.G. Jeong, J.H. Kwon, K.S. So, S.Y. Jeong, K.C. Choi. A review of highly reliable flexible encapsulation technologies towards rollable and foldable OLEDs. *J. Inf. Disp*. **2019**, *21*, 19–32. doi:10.1080/15980316.2019.1688694.

141 P. Kathirgamanathan, V. Arkley, S. Surendrakumar, Y.F. Chan, J. Antipan-Lara, S. Ganeshamurugan, M. Kumaraverl, G. Paramaswara, S. Ravichandran. Charge transporters for OLED's: strategies and performance. *SID Symp. Digest Tech. Papers*. **2008**, *39*, 701–704.

142 G.F. He, M. Pfeiffer, K. Leo, M. Hofmann, J. Birnstock, R. Pudzich, J. Salbeck. High-efficiency and low-voltage *p-i-n* electrophosphorescent organic light-emitting diodes with double-emission layers. *Appl. Phys. Lett*. **2004**, *85*, 3911–3913.

143 J. Kido (2008). High performance OLEDs for displays and general lighting. In: *SID Symposium Digest of Technical Papers*. Los Angeles, CA. 931–932.

144 A.B. Chwang, R.C. Kwong, J.J. Brown. Graded mixed-layer organic light-emitting devices. *Appl. Phys. Lett*. **2002**, *80*, 725–727.

145 F. Lindla, M. Boesing, C. Zimmermann, F. Jessen, P. Van Gemmern, D. Bertram, D. Keiper, N. Meyer, M. Heuken, H. Kalisch, R.H. Jansen. Highly efficient yellow organic light emitting diode based on a layer-cross faded emission layer allowing easy color tuning. *Appl. Phys. Lett*. **2009**, *95*, 213305.

146 S.-M. Sangmin, C.W. Lee, Tang, L.J. Rothberg (2012). Improved blue phoesphorescent OLEDs with a linearly-graded mixed-host architecture. In: *SID Symposium Digest of Technical Papers*. Boston, MA. 441–444.

147 C.-S. Chuang, J.-L. Cheng, S.-A. Chen, C.H. Chen (2011). Lifetime enhancement by fabrication of a doped graded-emission layer in organic light-emitting diodes. In: *SID Symposium Digest of Technical Papers*. Los Angeles, CA. 1080.

148 K. Walzer, B. Maennig, M. Pfeiffer, K. Leo. Highly efficient organic devices based on electrically doped transport layers. *Chem. Rev*. **2007**, *107*, 1233–1271.

149 J.S. Huang, M. Pferffer, A. Werner, J. Blochwitz, K. Leo, S. Liu. Low-voltage organic electroluminescent devices using pin structures. *Appl. Phys. Lett*. **2002**, *80*, 139–141.

150 J. Blochwitz, T. Fritz, M. Pfeiffer, K. Leo, D.M. Alloway, P.A. Lee, N.R. Armstrong. Interface electronic structure of organic semiconductors with controlled doping levels. *Org. Electron*. **2001**, *2*, 97–104.

151 L.S. Hung, C.W. Tang, M.G. Mason, P. Raychaudhuri, J. Madathil. Application of an ultrathin LiF/Al bilayer in organic surface-emitting diodes. *Appl. Phys. Lett*. **2001**, *78*, 544–546.

152 R. Meerheim, B. Lussem, K. Leo. Efficiency and stability of *p-i-n* type organic light emitting diodes for display and lighting applications. *Proc. IEEE*. **2009**, *97*, 1606–1626.

153 A. Dodabalapur, L.J. Rothberg, R.H. Jordan, T.M. Miller, R.E. Slusher, J.M Phillips. Physics and applications of organic microcavity light emitting diodes. *J. Appl. Phys*. **1996**, *80*, 6954.

154 S. Dirr, S. Wiese, H.-H. Johannes, W. Kowalsky. Organic electro- and photoluminescent microcavity devices. *Adv. Mater*. **1998**, *10* (*2*), 167–171.

155 G. Tan, J.-H. Lee, S.-C. Lin, R. Zhu, S.H. Choi, S.T. Wu. Systematic optimization for achieving indistinguishable color shifts of RGB OLED displays. *SID Symp. Digest Tech. Papers*. **2018**, *49* (*1*), 418–421.

156 S.F. Hsu, C.-C. Lee, A.T. Hu, C.H. Chen. Fabrication of blue top-emitting organic light-emitting devices with highly saturated color. *Curr. Appl. Phys*. **2004**, *4*, 663–666.

157 W. Song, J. You, C.-Y. Wu, L. Wang, Y. Shen, B. Bo, W. Quan, C. Luo, D. Yu, W. Li, H.T. Shih. 3-Stacked top emitting white OLEDs with super-wide color gamut and high efficiency. *Digest Int. Symp. SID*. **2019**, *50* (*1*), 45.

158 M.C. Gather, A. Köhnen, K. Meerholz. White organic light-emitting diodes. *Adv. Mater*. **2011**, *23*, 233–248.

159 J. Kido, T. Matsumoto, T. Nakada, J. Endo, K. Mori, N. Kawamura, A. Yokoi (2003). High efficiency organic EL devices having charge generation layers. In: *SID Symposium Digest of Technical Papers*. Baltimore, MD. 964–965.

160 L.S. Liao, K.P. Klubek, C.W. Tang. High efficiency tandem organic light-emitting diodes. *Appl. Phys. Lett*. **2004**, *84*, 167–169.

161 C.-C. Chang, S.-W. Hwang, C.H. Chen, J.F. Chen. High-efficiency organic electroluminescent device with multiple emitting units. *Jpn. J. Appl. Phys*. **2004**, *43*, 6418.

162 Y.H. Son, J.M. Lee, B.Y. Kang, J.H. Kwon. High efficiency three-stack tandem white OLEDs. *SID Symp. Digest Tech. Papers*. 2015, *46* (*1*), 561–563.

163 L.S. Liao, X. Ren, W.J. Begley, Y.S. Tyan, C.A. Pellow (2008). Tandem white OLEDs combining fluorescent and phosphorescent emission. In: *SID Symposium Digest of Technical Papers*. Los Angeles, CA. 818–821.

164 A. Sempel, M. Büchel. Design aspects of low power polymer/OLED passive-matrix displays. *Org. Electron*. **2002**, *3*, 89–92.

165 Z. Hara, K. Maeshima, N. Terazaki, S. Kiridoshi, T. Kurata, T. Okumura, Y. Suehiro, T. Yuki (2010). The high performance scalable display with passive OLEDs. In: *SID Symposium Digest of Technical Papers*. Seattle, WA. 357–360.

166 J.-J. Lih, C.-F. Sung, C.-H. Li, T.H. Hsiao, H.H. Lee. Comparison of a-Si and poly-Si for AMOLED displays. *J. Soc. Inf. Disp*. **2004**, *12* (*4*), 367–371.

167 H.D. Kim, J.K. Jeong, H.-J. Chung, Y.G. Mo (2008). Technological challenges for large-size AMOLED display. In: *SID Symposium Digest of Technical Papers*. Los Angeles, CA. 291–294.

168 G.R. Chaji, S. Alexander, A. Nathan, C. Church, S.J. Tang (2007). A low-cost stable amorphous silicon AMOLED display with full VT- and VOLED shift compensation. In: *SID Symposium Digest of Technical Papers*. Long Beach, CA. 1580–1583.

169 M. Miyasaka, J. Stoemenos. Excimer laser annealing of amorphous and solid-phase crystallized silicon films. *J. Appl. Phys*. **1999**, *86*, 5556–5565.

170 J.W. Hamer, A. Yamamoto, G. Rajeswaran, S.A. Van Slyke (2005). Mass production of full-color AMOLED displays. In: *SID Symposium Digest of Technical Papers*. Boston, MA. 1902–1907.

171 J.B. Choi, W.-K. Lee, Y.J. Chang, J.H. Oh, S.H. Jin, C.H. Park, B.K. Choo, I.D. Chung, K.H. Lee, H.B. Hwang, Y.S. Lee (2010). 30'' AMOLED based on sequential lateral solidification process. In: *SID Symposium Digest of Technical Papers*. Seattle, WA. 794–797.

172 Y. Matsueda, D.-Y. Shin, H.-K. Chung (2008). AMOLED technologies for uniform image and sufficient lifetime of image sticking. In: *SID Symposium Digest of Technical Papers*. Los Angeles, CA. 9–12.

173 P. Gong, H.G. Li. A novel compensation circuit for AMOLED source driver. *Digest Int. Symp. SID*. **2019**, *50* (*1*), 1026–1029.

174 H.J. Kim, K. Park, H.J. Kim. High-performance vacuum-processed metal oxide thin-film transistors: a review of recent developments. *J. Soc. Inf. Disp*. **2020**, *28*, 1–32.

175 Y. Takeda, S. Kobayashi, S. Murashige, K. Ito, I. Ishida, S. Nakajima, H. Matsukizono, N. Makita. Development of high mobility top gate IGZO-TFT for OLED display. *Digest Int. Symp. SID*. **2019**, *50* (*1*), 516–519.

176 T. Kamiya, K. Nomura, H. Hosono. Present status of amorphous In–Ga–Zn–O thin-film transistors. *Sci. Technol. Adv. Mater*. **2010**, 11, 044305.

177 L. Wang, C. Ruan, H. Xu, M. Le, J. Zou, H. Tao, L. Zhou, J. Pang, L. Lan, H. Ning, W. Wu. Flexible AMOLED based oxide TFT with high mobility. *Digest Int. Symp. SID*. **2017**, *48* (*1*), 342–344.

178 D.D. Han, Y. Zhang, Y.Y. Cong, W. Yu, X. Zhang, Y. Wang. Fully transparent flexible tin-doped zinc oxide thin film transistors fabricated on plastic substrate. *Sci. Rep-Uk*. **2016**, *6*, 38984.

179 T.-K. Chang, C.-W. Lin, S. Chang. LTPO TFT technology for AMOLEDs. *Digest Int. Symp. SID*. **2019**, *50* (*1*), 545–548.

180 T. Kamiya, H. Hosono. Roles of hydrogen in amorphous oxide semiconductor. *ECS Trans*. **2013**, *54* (*1*), 103.

181 Y. Iwasaki, H. Fukagawa, T. Shimizu. Operationally stable blue inverted OLEDs employing fluorescent emitter. *SID Symp. Digest Tech. Papers*. **2019**, *50* (*1*), 1873–1876.

182 T. Sasaki, H. Fukagawa, T. Oono, K. Kuwada, M. Hasegawa, K. Morii, T. Shimizu. Demonstration of long-term stable emission from inverted OLED with imperfect encapsulation. *Digest Int. Symp. SID*. **2018**, *40* (*1*), 811–814.

183 N. Nakamura, T. Watanabe, J. Kim, S. Watanabe, E. Matsuzaki, Y. Toda, N. Miyakawa, S. Fujitsu, H. Hosono. Deposition and structuring processes of a newly developed transparent amorphous oxide semiconductor for the electron transport and injection layers of AM-OLEDs. *SID Symp. Digest Tech. Papers*. **2015**, *46* (*1*), 1710–1713.

184 Y. Zhou, C. Fuentes-Hernandes, J. Shim, J. Meyer, A.J. Giordano, H. Li, P. Winget, T. Papadopoulos, H. Cheun, J. Kim, M. Fenoll. A universal method to produce low-work function electrodes for organic electronics. *Science*. **2012**, *336*, 327–332.

185 J.K. Noh, M.S. Kang, J.S. Kim, J.H. Lee, Y.H. Ham, J.B. Kim, S. Son. Inverted OLED. *SID Symp. Digest Tech. Papers*. **2008**, *39* (*1*), 212.

186 M. Nakata, G. Motomura, Y. Nakajima, T. Takei, H. Tsuji, H. Fukagawa, T. Shimizu, T. Tsuzuki, Y. Fujisaki, T. Yamamoto. Development of flexible displays using back-channel-etched In–Sn–Zn–O TFTs and air-stable inverted OLEDs. *SID Symp. Digest Tech. Papers*. **2015**, *46* (*1*), 969–972.

187 C.-Y. Wu, M.-H. Ho, S.-M. Gao. et al. Efficient and color-saturated inverted bottom-emitting organic light-emitting devices with a semi-transparent metal-assisted electron injection layer. *Digest Int. Symp. SID*. **2009**, *40* (*1*), 1673–1676.

188 R. Young. The outlook for OLED remains bright. *Inf. Displ*. **2020**, *36*, 41–45.

189 *Display Search* OLED lighting in 2019 and beyond: The Bright Future.

190 R.M. Soneira (2020). Galaxy S20 ultra OLED display technology shoot-out. http://www.displaymate.com/Galaxy_S10_ShootOut_1S.htm.

191 J. Donelan. The 2019 display industry awards. *Inf. Displ*. **2019**, *35*, 20–58.

192 J. Donelan. The display industry awards: honoring creativity at its best. *Inf. Disp*. **2020**, *36*, 10–15.

193 K. Werner. Six CES headlines worth following. *Inf. Disp*. **2020**, *36*, 43–47.

194 M. Hack, M.S. Weaver, J.J. Brown. Status and opportunities for phosphorescent OLED lighting. *Digest Int. Symp. SID*. **2017**, *48* (*1*), 187–190.

195 C.-W. Han, H.K. Kim, H.S. Pang, S.H. Pieh, C.J. Sung, H.S. Choi, W.C. Kim, M.S. Kim, Y.H. Tak. Dual-plate OLED display (DOD) embedded with white OLED. *J. Displ. Technol*. **2009**, *5*, 541–545.

196 C.-W. Han, M.-Y. Han, S.-R. Joung, J.S. Park, Y.K. Jung, J.M. Lee, H.S. Choi, G.J. Cho, D.H. Kim, M.K. Yee, H.G. Kim. 3 Stack-3 color white OLEDs for 4K premium OLED TV. *Digest Int. Symp. SID*. **2017**, *48*, 1.

197 J.Y. Noh, D.M. Han, W.C. Jeong, J.W. Kim, S.Y. Cha. Development of 55" 4K UHD OLED TV employing the internal gate IC with high reliability and short channel IGZO TFTs. *J. Soc. Inf. Disp*. **2018**, *26* (*1*), 36–41.

198 H.-J. Shin, S. Takasugi, K.-M. Park, S.H. Choi, Y.S. Jeong, B.C. Song, H.S. Kim, C.H. Oh, B.C. Ahn. Novel OLED display technologies for large-size UHD OLED TVs. *Digest Int. Symp. SID*. **2015**, *46*, 53–56.

199 S. Takasugi, H.-J. Shin, M.-K. Chang, S.M. Ko, H.J. Park, J.P. Lee, H.S. Kim, C.H. Oh. Advanced compensation technologies for large-sized UHD OLED TVs. *J. Soc. Inf. Disp*. **2016**, *24* (*7*), 410–418.

200 S. Lee, K. Park, S. Park, J. Lee, H. Park. Improved sound quality by using the exciter speaker in OLED panel. *J. Soc. Inf. Disp*. **2020**, *28*, 297–307.

201 S.H. Hwang, Y.J. Kang, Y.W. Kim, H.J. Noh, T.W. Ko, S.D. Roh, S.H. Choi, C.S. Lim, Y.H. Shin, J.M. Kim, C.H. Oh. Study on the efficiency improvement of OLED TVs with high transmittance technology of the polarizer. *Digest Int. Symp. SID*. **2019**, *50*, 850–852.

202 K. Werner. The best of CES 2019. *Inf. Disp*. **2019 Jan/Feb**, 32.

203 J. Fu, T. Wu, X. Chi, X. Xia, Z. He. The novel transparent display based on IGZO TFTs with high transmittance and low reflectance. *Int. Conf. Disp. Technol (ICDT)*. **2019**, *50* (*S1*), 422–427.

204 S. Shama, U. Jindal, M. Goyal, S. Sharma, V. Goyal. A review on different types of displays. *Int. J. Multimed. Ubiquitous Eng*. **2016**, *11* (*8*), 337.

205 J.W. Kim, W.J. Choe, K.H. Hwang, J.O. Kwag. The optimum display for virtual reality. *Digest Int. Symp. SID*. **2017**, *48* (*1*), 1146–1149.

206 C. Vieri, G. Lee, N. Balram, S.H. Jung, J.Y. Yang, S.Y. Yoon, I.B. Kang. An 18 megapixel 4.3″ 1443 ppi 120 Hz OLED display for wide field of view high acuity head mounted displays. *J. Soc. Inf. Disp*. **2018**, *26* (*5*), 314–324.

207 Z. Bouhamri, E. Virey, P. Mukish. Can we overcome the challenges on the path to consumer adoption of AR headsets? *Digest Int. Symp. SID*. **2019**, *50* (*1*), 109–111.

208 A. Ghosh, I. Khayrullin, Q. Wang, F. Vazan, T. Ali, I. Wacyk, K. Tice, L. Sziklas. OLED micro-displays for VR/AR applications. *Digest Int. Symp. SID*. **2019**, *50* (*1*), 26–27. *US Patent 10644239and US 10636969* (2020).

209 G. Phelan. OLED lighting hits the market. *Inf. Disp*. **2018**, *34* (*1*), 10–15.

210 J.D. Bullough, S. Peana. Investigating blue-light exposure of lighting and displays. *Inf. Disp*. **2019**, *36*, 17–20.

211 U.S. Department of Energy, OLED Lighting Performance (2019). *Lighting R&D Opportunities*. 29.

212 Y.S. Tyan, Y.Q. Rao, X.F. Ren, R. Kesel, T.R. Cushman, W.J. Begley, N. Bhandari. Tandem hybrid white OLED devices with improved light extraction. *Digest Int. Symp. SID*. **2009**, *40* (*1*), 895–898.

213 A. Tanaka, H. Etori, R. Hayakawa. High performance outcoupling film for OLEDs lighting. *Int. Manuf. Inf. Disp. (IMID) Korea*. **2016**, *25* (*3*), 108.

214 S.-H. Eom, E. Wrzesniewski, J. Xue. Close-packed hemispherical microlens arrays for light extraction enhancement in organic light-emitting devices. *Org. Electron*. **2011**, *12*, 472–476.

215 Y. Qu, M. Slootsky, S.R. Forrest. *Nat. Photonics*. **2015**, *9*, 758.

216 H.K. Ham, Y.T. Oh, S.E. Choi, J.W. Park, B. Choi, D.C. Shin. Out-coupling efficiency enhancement of organic light emitting diode device by SiO_2-UV hardener composite layer. *J. Nanosci. Nanotechnol*. **2011**, *11*, 1766.
217 A. Mikami, T. Goto. Optical design of enhanced light extraction efficiency in multi-stacked OLEDs coupled with high refractive-index medium and back-cavity structure. *Digest Int. Symp. SID*. **2012**, *43* (*1*), 683.
218 H. Lu, J.-H. Jou, Y.-C. Xu, G.Y. Huang, L.-N. Gong, C.-C. Lo, J.-H. Chen. High efficiency internal extraction substrate for OLED lighting. *Digest Int. Symp. SID*. **2019**, *50* (*1*), 58.
219 J. Donelan. LG display intensifies OLED lighting push. *Inf. Disp*. **2018**, *34* (*1*), 3.
220 https://www.oled-info.com/lg-mass-production-5-gen-lighting-oled-gumi-30x.
221 J. Spindler, M. Kondakova, M. Boroson, M. Büchel, J. Eser, J. Knipping. Advances in high efficacy and flexible OLED lighting. *Digest Int. Symp. SID*. **2018**, *49* (*1*), 1135.
222 N. Ohsawa, S. Idojiri, K. Kumakura, S. Obana, Y. Kobayashi, M. Kataniwa, T. Ohide, M. Ohno, H. Adachi, N. Sakamoto, S. Yatsuzuka. Large-sized flexible lighting with highly efficient OLEDs. *Digest Int. Symp. SID*. **2013**, *44* (*1*), 923.
223 H. Bechert, S. Wittmann, C.J. Brabec, T. Wehlus. Flexible and highly segmented OLED for automotive applications. *Proc. SPIE*. **2018**, *106870*, Q-1-9.
224 https://www.spiegel.de/auto/fahrberichte/audi-a8-im-test-neue-generation-der-oberklasse-limousine-a-1171221.html.
225 M. Kruppa, W. Thomas, W. Huhn. An OLED taillight revolution: from point light sources to segmented area light sources. *Inf. Disp*. **2019**, *35* (*2*), 14.
226 E.A. Margulies, P.T. Boudreault, V.I. Adamovich, B.D. Alleyne, M.S. Weaver, J.J. Brown. Narrow spectrum deep red emitters for OLED lighting and display. *Digest Int. Symp. SID*. **2019**, *50* (*1*), 911.
227 Y. Zhu, L. Guo, Y. Lee, X. Xu , J. Xie , G. Zhang, Y. Hu. OLED in automotive lighting applications. *Digest Int. Symp. SID*. **2019**, *50* (*1*), 628.